ORIGINAL ARTICLE

Eur J Anat, 15 (1): 47-72 (2011)

A rat model of oligomeric forms of beta-amyloid (Aß) peptide: neuronal loss, synaptic alteration, astrogliosis, and calcium-binding proteins activation in vivo

Alicia Gonzalo-Ruiz[1], Maria Delso[1], Isabel Carrero[1], Pilar Gonzalo Vicente[1], José Miguel Sanz-Anquela[2], Manuel Rodríguez[3], Juan Arévalo-Serrano[2]

1. *Laboratory of Neuroanatomy, Institute of Neuroscience of Castilla and León, University of Valladolid (Campus "Duques de Soria"), 42004-Soria, Spain.*
2. *Department of Medicine, Hospital Príncipe de Asturias, Alcalá de Henares, Madrid, Spain*
3. *Department of Biochemistry, University of Barcelona, Spain.*

SUMMARY

Oligomers of Beta-amyloid (Aß) peptide are presumed to cause synaptic and cognitive dysfunction in Alzheimer's disease (AD). However, their contribution to other pathological features of AD remains unclear. To address the latter, we applied microinjections of Aß1-42 oligomers into the retrosplenial cortex of the rat. We observed that Aß1-42 induced a greater reduction in neuronal density as compared with that seen at control (Aß42-1) injections. Oligomers of Aß1-42 peptide caused synaptic alterations, as evidenced by the decrease in the presynaptic marker synaptophysin and the increase in chromogranin A. We also detected a marked interaction between GFAP-, and Aß-immunoreactive material in a time-dependent manner. To address the possible mechanisms involved in astrocyte activation, we analyzed the interaction between the calcium-dependent protease, calpain-1, and the calcium-binding protein, S100B, and astrogliosis in response to Aß toxicity. Calpain-1 activation was studied by immunoblotting. Three immunopositive protein bands (80kDa, 76kDa, and 18kDa) were detected. Densitometry analyses revealed a significant increase in calpain-1 at 76kDa and at position 18kDa in Aß1-42-treated animals as compared with the corresponding bands in control animals. Confocal analysis showed codistribution of Aß-, and calpain 1-immunoreactivities in cortical cells, and in reactive astrocytes surrounding the injection of Aß, and both cortical and leptomeningeal blood vessels. A co-localization of GFAP and S100B proteins was observed in astrocytes that surrounded the Aß injection, and also in reactive astrocytes in close association with blood vessels. In conclusion, our results suggest that calpain-1 and S100B might play a critical role in astroglisois in response to Aß toxicity.

Key words: Alzheimer's disease – Retrosplenial cortex – Astrocytosis – S100B – Calpain-1

Submitted: December 3, 2010
Accepted: January 7, 2011

Corresponding author:
Dr. Alicia Gonzalo-Ruiz. Laboratory of Neuroanatomy, Institute of Neuroscience of Castilla and León, University of Valladolid, Campus "Duques de Soria", 42004-Soria, Spain. Phone: 34 975 129184; Fax: 34 975 129101. E-mail: agruiz@ah.uva.es

Introduction

Alzheimer's disease (AD) is a neurodegenerative disease characterized by a progressive memory loss and cognitive decline (HSelkoe, 2002H). The pathological hallmarks of AD are extracellular plaques containing amyloid-ß (Aß), dystrophic neurites, activated microglia, reactive astrocytes and synapse loss (Selkoe and Schenk, 2003). In v*itro* and *in vivo* studies have supported the amyloid cascade hypothesis, in which the seeding of insoluble Aß1-42 is a causative factor in the pathogenesis of AD (HHardy and Selkoe, 2002H). However, amyloid plaques do not always correlate with neurodegeneration and cognitive decline (HMucke et al 2000H).

There are clear indications that increased levels of soluble Aß is the primary cause of neuronal pathology in AD (Haass and Selkoe, 2007; Klein, 2002; Walsh and Selkoe, 2007). *In vivo*, small stable oligomers of Aß1-42 have been isolated from the brain of AD patients (HGong et al., 2003H), and the levels of soluble Aß are well correlated with synaptic dysfunction (Kokubo et al., 2005; Lacor et al., 2007, Selkoe, 2008; Walsh et al., 2002), and cognitive deficits (Cleary et al 2005; Lesné et al., 2006) in the AD brain. Recently, the oligomeric and protofibrillar forms of Aß have been the subject of numerous studies employing a variety of experimental approachesH (HHernández et al., 2010; Oddo et al., 2006; Perez et al., 2010, Tomiyama et al., 2010). In addition, there is extensive evidence that exogenous application of synthetic Aß peptide or oligomeric aggregates leads to a rapid and aberrant regulation of Ca^{2+} homeostasis, resulting in structural and functional disruption of neuronal networks (Berridge, 2010; HDemuro et al., 2005H; Ferreiro et al., 2008; Resende et al., 2007; 2008). Calcium dysregulation, in turn, increases calpain activation, as seen in post mortem human AD patients' brains (Nixon et al., 1994; Saito et al., 1993; Vosler et al., 2009; Wu et al., 2007). Alterations in calpain activation associated with calcium homeostasis have also been proposed to play an important role in the degeneration of neurons (Adamec et al., 2002; Lebart and Benyamin, 2006; HNixon, 2003H), as well as in reactive astrocytes (Gray et al., 2006; Lee et al., 2000).

Accumulating evidence also indicates that Aß induces the glial-mediated inflammatory response that contributes significantly to cognitive decline and oxidative stress-dependent neurodegeneration (HAkiyama et al., 2000;H Griffin et al., 1998; McGeer and McGeer, 2001; Meda et al., 2001). Past research has focused on Aß plaque-associated activated microglia because of their well documented roles in exacerbating or mitigating AD pathology (Akiyama, 2000; Town et al., 2005). However, recent evidence suggests that activated astrocytes may play a dichotomous role in several brain pathologies, including AD (Domenici et al., 2002; Johnstone et al., 1999; Malchiodi-Albedi et al., 2001; Rodriguez et al., 2009; Simpson et al., 2010). Reactive astrocytes are normally characterized by an overexpression of the glial fibrillary acidic protein (GFAP), the major component of the astrocytic cytoskeleton (Reymond et al., 1996; Ridet et al., 1997). Importantly, astrocyte activation, seen in an increase in the expression of GFAP, has been observed after exogenous application of oligomers of Aß peptide (Perez et al., 2010), and proteomic analyses have revealed a complex GFAP pattern, with different patterns of modification and degradation (Korolainen et al., 2005; Perez et al., 2010; Riederer et al., 2009). Little is known, however, about the precise mechanism(s) by which the expression of GFAP is increased in response to exogenous application of oligomers of Aß peptide.

Based on our previous results (Pérez et al., 2010), together with increasing evidence supporting the functional importance of calcium (Ca^{2+})-mediated astrocyte activation (Araque et al., 2001; Mattson and Chan, 2003; Takuma et al., 2004) and the fact that the Ca^{2+}-binding protein, S100B, and the Ca^{2+}-dependent protease, calpain-1, are thought to play a pivotal role in reactive astrocytes (Donato, 2001; Gray et al., 2006; Lee y cols., 2000), we draw this study to determine, in addition to the neuronal loss and the synaptic alterations in the early stages of Aß toxicity, the expression of calpain-1 and S100B proteins in reactive astrocytes in response to microinjections of Aß1-42 oligomers into the restrosplenial cortex of the posterior cingulate gyrus, a key brain region intimately involved in learning and memory processes (Albasser et al., 2007; Lukoyanov and Lukoyanova, 2006; Nestor et al., 2003; Vann and Aggleton, 2002). In order to analyze further the specificity of Aß1-42 peptide, the reversible form

of Aß1-42 (Aß42-1 peptide) was used as a control. This study should provide insight into the discrete and perhaps early mechanisms through which astrocytes are stimulated to acquire a reactive phenotype in response to Aß peptide.

Materials and Methods

Experimental animals and anaesthesia

Female Wistar rats (n = 64; 250 to 300g) were used. They were kept under standard laboratory conditions (20ºC ambient temperature, 12 h light/dark cycle, tap water and regular rat chow *ad libitum*). All possible efforts were made to minimize animal suffering and to reduce the number of animals used. All animals were anaesthetised with equitesine (0,33ml/100g, injected intraperitoneally) for the surgical procedure (injection of either Aß1-42 peptide or its reverse sequence Aß42-1). Prior to perfusion with fixative, all animals were re-anaesthetized in the same manner, but with up to double the dose used for the surgical procedure. In each case the animals were housed and handled according to Spanish legislation and the guidelines approved by the Animal Care Committee of the University of Valladolid, which comply with, or are even more stringent than Spanish Directive 1201/2005 and European Directive 86/609.

Preparation of Aß oligomers

Aß1-42 oligomers were prepared as reported previously (Klein, 2002), following the protocol described by Perez et al. (2010). In brief, Aß1-42 (Bachem) was initially dissolved to 1mM in hexafluoroisopropanol and separated into aliquots in sterile microcentrifuge tubes. Hexafluoroisopropanol was removed under vacuum in a speed vac., and the peptide film was stored desiccated at -20°C. For the aggregation protocol, the peptide was first resuspended in dry dimethyl sulfoxide at a concentration of 5 mM and then, for the preparation of oligomers, Ham's F-12 was added to bring the peptide to a final concentration of 100 µM; this was incubated at 4°C for 24 h. The preparation was then centrifuged at 14,000µg for 10 min at 4°C to remove insoluble aggregates (protofibrils and fibrils) and the supernatants containing soluble Aß1-42 oligomers were transferred to clean tubes and stored at 4°C. Aß42-1 peptide (Bachem) was prepared following the protocol described above for preparation of Aß1-42 oligomers.

Western blot analysis of samples of Aß1-42 and Aß42-1 peptides

Western blotting was performed as described earlier (Perez et al., 2010). In brief, a standard 15% PAGE-SDS was prepared and 5 µl samples of either Aß1-42 oligomers or Aß42-1 at a 100 µM concentration were incubated with 1X loading buffer. The samples were loaded in the gel without boiling, after which the gel was run at constant amperage of 40 mA and transferred to nitrocellulose. The membranes were blocked for 1h in a solution of 5% nonfat-dry milk in TBS-T, and then incubated with either 6E10 (1:800), a mouse monoclonal Aß antibody to residues 1-17 (Sigma), *or* 4G8 (1:800), a mouse monoclonal Aß antibody to residues 17-24 (Sigma). After incubation with the primary antibody, the membranes were washed in TBS-T and then incubated with HRP-conjugated secondary antibodies. The blots were washed again, followed by detection with an enhanced chemiluminescence (ECL) kit (GE Healthcare) and exposed to films. Molecular masses were estimated by Rainbow molecular weight markers (Bio-Rad).

Injection of either Aß1-42 oligomers or Aß42-1 sequence peptide

The anaesthetized animals (n = 64) were placed in a stereotaxic frame. A hole was made in the parietal bone with a dental drill and the dura was opened with a fine hypodermic needle. In one group of animals (n = 36), under equitesine anaesthesia, a single unilateral microinjection of Aß1-42 oligomers (BACHEM, at a concentration of 2µg) was performed in the left retrosplenial cortex, using stereotaxic coordinates derived from the atlas of Paxinos and Watson (1986). Oligomeric species of synthetic Aß1-42 peptide were prepared as described above, and reported previously by Perez et al. (2010). The dose of the Aß protein was selected on the basis of our previous studies (Arévalo-Serrano et al., 2008; Gonzalez et al., 2008). All microinjections were administered using a 10µl Hamilton syringe with a 26 -gauge stainless steel needle, which was slowly lowered into place. The needle was left in place for 3-5 min before the injection was started, after which the fragments were injected slowly at a rate of 0.2µl/min. The needle was left in place

for an additional 3-5 min before being slowly withdrawn. As a control, in a second group of animals (n = 28), also under equitesine anaesthesia and using a different microsyringe, a single unilateral microinjection of Aß42-1 peptide (BACHEM, 2µg) was administered into the corresponding regions of the left retrosplenial cortex. After the injection, the scalp was sutured and the animals were allowed to recover from the anaesthetic.

Immunocytochemical and immunofluorescence studies

Fixation

Following post-injection survival periods of 24h, 72h, 7d, and 14d, one group of animals [(n = 32), Aß1-42 treated animals, n = 20, 5 animals/each time period; Aß42-1/control group, n = 12, 3 animals/each time period] were re-anaesthetized and the brain tissue was fixed by intracardiac perfusion of 60 ml of 0.9% saline at 20ºC containing heparin (1.000 IU) to flush blood from the vascular system, followed by ca 350-400 ml of fixative solution containing 4% paraformaldehyde and 0.1% glutaraldehyde in 0.1M phosphate buffer (PB) at pH 7.2 (also perfused at 20ºC).

Tissue preparation, histochemical, and immunohistochemical procedures

Immediately after perfusion, the brain was removed, trimmed, sectioned in the coronal plane at 40µm using a freezing microtome, and collected serially as several series of adjacent sections. All sections were stored under similar conditions at 4ºC (between 1 and 10 days) before they were processed for histochemical and immunocytochemical methods. In one group of Aß1-42 injected animals (n = 20) and in the control animals (n = 12) a series of adjacent sections, which contained the full antero-posterior extent of the injection site, were mounted on gelatinized slides and stained with 0.1% cresyl violet to identify the injection site, the area of toxicity, and to visualize neuronal nuclei and perikarya. Another series of sections that also contained the full antero-posterior extent of the injection site was processed for single antigen localization of the Aß peptide (Method 1). A further series of adjacent sections, which contained the full antero-posterior extent of the injection site as well as the full antero-posterior extent of the hippocampus, temporal, frontal, and entorhinal cortices, were processed for the sequential double-immunohistochemical or double-immunofluorescence localization of Aß and glial fibrillary acid protein (GFAP), Aß and synaptophysin, Aß and chromogranin A, Aß and calpain-1, GFAP and calpain-1, and GFAP and S100B (Method 2).

Method 1: Single-labelling immunohistochemistry (Aß)

Immunostaining was performed on free-floating sections. Sections processed for the immunohistochemical localization of Aß peptide were first immersed for 1 h in 10% normal goat serum (NGS) in 0.01M phosphate-buffered saline (PBS) containing 0.3% Triton X-100 and 0.1 M lysine. After rinsing in PBS, endogenous peroxidase activity was blocked with 1% hydrogen peroxide (H_2O_2) in PBS for 30 min. The sections were then incubated in a solution containing a mouse monoclonal antibody against Aß (CLONE: 6E10, 1:1000 dilution; Sigma-Aldrich) for 18-24h at 4ºC. After incubation in the primary antibody, the sections were washed in 1% NGS and then incubated in biotinylated goat anti-mouse IgG (Vector, 1:200 in PBS with 1% NGS) and immersed in an avidin: biotin-HRP complex (Vector, 1:100 dilution) for 60 min. The immunoreaction product was visualized using 0.005% DAB and 0. 01% H_20_2 in PB. The sections were rinsed through several changes of PB, mounted on gelatinized microscope slides, air-dried, dehydrated, covered with Permount, and examined and photographed under bright-field illumination.

As a control, some sections were incubated as described above but without the addition of primary antibody or after replacing the primary antibody with normal goat serum. There was a complete absence of Aß-immunoreactivity in such control sections.

Single-labelling immunofluorescence (Neuronal nuclei, NeuN)

Sections processed for the immunohistochemical localization of NeuN protein were first immersed for 1 h in 10% normal goat serum (NGS) in 0.01M phosphate-buffered saline (PBS) containing 0.3% Triton X-100 and 0.1 M lysine. After a rinse in PBS, endogenous peroxidase activity was blocked with 1% hydrogen peroxide (H_2O_2) in PBS for 30 min. The sections were then incubated in a solution containing a mouse anti-NeuN monoclonal antibody (1:100 dilution;

CHEMICON, Int) for 18-24h at 4ºC. After incubation in the primary antibody, the sections were washed in 1% NGS and then incubated in biotinylated goat anti-mouse IgG (Vector, 1:200 in PBS with 1% NGS). Sections were then washed in PBS and incubated using fluorescein (FITC)-conjugated avidin D (Vector, 1:100 in PBS).

Method 2: Double-labelling immunohistochemistry (e.g., Aß/calpain-1, GFAP/calpain-1, Aß/synaptophysin, Aß/chromogranin A)

The sections processed for the sequential double-immunohistochemical localization of Aß/chromogranin A, Aß/calpain-1, and **GFAP**/calpain-1 were first immersed for 1h in 10% normal goat serum (NGS) in PBS containing 0.3% Triton X-100 and 0.1 M lysine. After a rinse in PBS, endogenous peroxidase activity was blocked with 1% H_2O_2 in PBS for 30 min, after which the sections were rinsed in PBS again. Sections processed for the immunohistochemical localization of Aß and GFAP were then incubated in a solution containing mouse monoclonal antibodies against Aß (CLONE: 6E10, 1:1000 dilution; Sigma-Aldrich) or against GFAP (1:3500 dilution, Sigma-Aldrich) for 18-24h at 4ºC. After incubation in the primary antibody, the sections were washed in 1% NGS and then incubated in biotinylated goat anti-mouse IgG (1:200 in PBS with 1% NGS). The sections were then washed in PBS and immersed in avidin-biotin-HRP complex (1:100 dilution) for 60 min. The immunoreaction product was visualized using 0.005% DAB and 0.01% H_2O_2 in PB. After immunostaining, the sections were rinsed in PBS over a period of 60 min. The sections were then incubated with another primary antibody, against the second antigen, using goat polyclonal antibodies against chromogranin A (1: 100 dilution; Santa Cruz Biotechnology, Inc), or calpain-1 (1:200 dilution; Santa Cruz Biotechnology, Inc.) for 18-24h at 4ºC. After incubation with the primary antibody, the sections were washed in 1% normal rabbit serum (NRS) and then incubated in biotinylated rabbit anti-goat IgG (Vector, 1: 200 dilution in PBS with 1% NRS). The second antigen was then visualized with BDHC (Levey et al., 1986). This chromogen produced a blue-dark granular reaction product. After immunostaining, all sections were then rinsed through several changes of PB, mounted on gelatinized microscope slides, air-dried, dehydrated, covered with Permount, and examined and photographed under bright-field illumination.

As a control, some sections were processed for the two-colour co-localization procedure as described above, but without the addition of primary antibody or after replacing the primary antibody with normal serum respectively. Control sections were processed through the secondary antiserum, DAB, and BDHC steps in exactly the same way as the other sections. There was a complete absence of single- or double-labelling neurons or neuropil in such control sections.

Double-labelling immunofluorescence (e.g., Aß/calpain-1, Aß/GFAP, GFAP/calpain-1 Aß/chromogranin A, Aß/synaptophysin, GFAP/S100B)

First, the sections processed for the sequential double-immunohistochemical localization of Aß/calpain-1, Aß/GFAP, Aß/chromogranin A, and **GFAP**/calpain-1 were immersed for 1h in 10% NGS in PBS containing 0.3% Triton X-100 and 0.1M lysine, while those processed for sequential double-immunohistochemical localization of Aß/synaptophysin, and **GFAP**/S100B were immersed for 1h in 10% NRS in PBS containing 0.3% Triton X-100 and 0.1M lysine. Sections processed for the immunohistochemical localization of Aß were then incubated in a solution containing a mouse monoclonal antibody against Aß (CLONE: 6E10, 1:1000 dilution; Sigma-Aldrich), whereas those processed for GFAP were incubated in a solution containing mouse monoclonal antibody against GFAP (1:3500 dilution, Sigma-Aldrich) for 18-24h at 4ºC, and then incubated in biotinylated goat anti-mouse IgG (Vector, 1:200 in PBS with 1%NGS) for the immunolocalization of Aß/calpain-1, Aß/GFAP, Aß/chromogranin A, and **GFAP**/calpain-1, or in biotinylated rabbit-anti-mouse IgG (Vector, 1:200 in PBS with 1%NRS) for the immunolocalization of Aß/synaptophysin, and **GFAP**/S100B. Sections were then washed in PBS and incubated using either rhodamine-conjugated avidin D (Vector, 1:100 in PBS) or fluorescein (FITC)-conjugated avidin D (Vector, 1:100 in PBS). The sections were rinsed in PBS for more than 60 min and then incubated with another primary antibody, against the second antigen, using either goat polyclonal antibodies against calpain-1 (1:200 dilution, Santa Cruz Biotechnology, Inc), chromogranin A

(1:100, Santa Cruz, Biotechnology, Inc), and GFAP (1:200, Santa Cruz, Biotechnology, Inc), or rabbit polyclonal antibodies against synaptophysin (1:200, Santa Cruz Biotechnology, Inc), and S100B (1:50, abcam) for 18-24h at 4ºC. After incubation in the primary antibody against the second antigen, the sections were washed either in 1% NRS (for Aß, chromogranin A, or calpain-1) or in 1% NGS (for synaptophysin or GFAP) and then incubated in biotinylated rabbit anti-goat IgG (Vector, 1:200 in PBS with 1% NRS) for the immunolocalization of Aß/**GFAP**, Aß/**chromogranin A,** Aß/**calpain-1**, and GFAP/**calpain-1**, or in biotinylated goat anti-rabbit IgG (Vector, 1:200 in PBS with 1%NGS) for the immunolocalization of Aß/**synaptophysin,** and GFAP/**S100B.** The second antigen was visualized using either fluorescein (FITC)-conjugated avidin D (Vector, 1:100 in PBS) or rhodamine-conjugated avidin D (Vector, 1:100 in PBS).

As control, some sections were processed for the two-colour co-localization procedure as described above, but without the addition of primary antibody or after replacing the primary antibody with the respective normal serum. Control sections were processed through the secondary antiserum, rhodamine and FITC steps, in exactly the same way as the other sections.

Analysis of the immunohistochemical material

In each series of sections stained immunocytochemically with antibodies against Aß, or double-labelled for Aß/GFAP, Aß/calpain-1, Aß/chromogranin-A, Aß/synaptophysin, GFAP/calpain-1, and GFAP/S100B, all sections through the full rostro-caudal extent of the injection site, the rostro-caudal extent of cerebral cortex, and the full rostro-caudal extent of the hippocampus (each separated by approximately 280µm) were examined systematically. Immunocytochemically-processed material was viewed under bright-field illumination with an Olympus microscope (BX50). The specificity of the immunoreaction was checked by comparing sections stained either with single antiserum (Aß) or double-labelled (e.g., Aß/calpain-1, GFAP/calpain-1) and control material, respectively. Structures immunostained by antibodies but not visualized in the control slides were considered to be specifically immunolabelled and here are designated as Aß-immunoreactive (IR). All single-IR and all double-labelled structures were scored at 20x magnifications using an ocular grid.

The double-fluorescence-labelled sections were examined with fluorescence microscope, and imaged using a confocal laser scanning imaging system attached to a microscope (Zeiss). Sections were illuminated by light with an excitation wavelength of 488 nm (argon laser) for FITC, and 568 nm (krypton laser) for rhodamine. Single and series of optical sections were transferred separately to channel 1 and channel 2 to avoid crosstalk, and then superimposed. Green and red images were acquired simultaneously and are either presented separately (e.g., Figs. 10A, B, 11A, B), or as a superimposed image (e.g., Figs.10C, 11C).

Terminal deoxynucleotidyl transferase-mediated by immunoperoxidase labelling (TUNEL) assay

The amount of apoptosis at the injection site of Aß1-42 peptide was determined by direct immunoperoxidase detection of digoxigenin-labelled genomic DNA in paraffin sections of fixed tissue. TUNEL assays were performed using the Oncor ApopTag peroxidase detection kit, which detects the 3'-OH region of cleaved DNA during apoptosis, and the protocol recommend by the manufacturer. Briefly, microsections were incubated with Proteinase K (20µg/ml) for 15 min. TUNEL reaction mixture was added, and the tissue incubated in a humidified chamber for 1h at 37ºC and then washed in PBS for 5 min at room temperature. The sections were then immersed in streptavidin-HRP complex, and the immunoreaction product was visualized using 0.005% DAB and 0.01% H_2O_2 in PB. Application of streptavidin-HRP allows the identification of apoptotic nuclei (dark brown colour) by light microscopy.

Western blotting of Aß peptide and calpain-1 activity in the rat brain

Small portions (around 200 mg) of frozen retrosplenial cortex of Aß1-42 treated animals (n = 16, 4 animals each time point) and control (Aß42-1) animals (n = 16, 4 animals/time point) were homogenized as described by Ramonet et al. (2004). The protein concentration was determined using the DC protein Assay kit (Bio-Rad). Homogenate volumes

with 10 µg of total protein were loaded in 15% gel, denatured by heating for 5 min at 100ºC, and then the gel was run at constant amperage of 40 mA. After electrophoresis, the proteins were transferred onto nitrocellulose membranes, which were blocked for 1 h with Tris-buffer-saline containing 0.1% Tween-20 (TBS-T, pH 7.5), and 5% non-fat dry milk. After washing in TBS-T, the nitrocellulose membranes were incubated in a solution containing mouse monoclonal antibodies against either Aß (CLONE 6E10,1:800 in TBS-T, Sigma) or calpain-1 (1:50 in TBS-T, Santa Cruz Biotechnology, Inc.) overnight at 4ºC. After incubation in the primary antibody, the membranes were washed in TBS-T and then incubated in biotinylated anti-mouse IgG (Vector, 1: 5000 in TBS-T) and immersed in ExtrAvidin peroxidase complex (Sigma, 1: 4000 in TBS-T) for 60 min. The immunoreactive Aß and calpain-1 proteins were detected using a chemiluminescence (ECL) kit (GE Healthcare) and were exposed to films. The films were developed, scanned, and analyzed by computer-assisted image analysis (UN-SCAN-IT digitizing software, Silk Scientific, Inc.). Molecular masses were estimated by Rainbow molecular weight markers (Bio-Rad). Student's *t* test analysis was used to assess the significance of differences between groups if normal distribution could be assumed. If the normality was not valid, statistical differences among groups were calculated by means of the non-parametric Mann-Whitney U-test.

Results

Characterization of Aß peptide in samples of both Aß1-42 and Aß42-1 peptide, and following Aß injections *in vivo* in the rat brain

As described in Material and Methods, we used the protocol reported by Klein (2002), and Perez et al. (2010) to prepare oligomers from Aß1-42 obtained from a commercial source (Bachem). Second, in order to confirm that the Aß1-42 peptide maintained the appropriate oligomeric conformation we characterized its quaternary structure using 15% SDS-PAGE gel. The size distribution of the sample of Aß1-42 oligomers was determined by Western blotting, using monoclonal antibodies against Aß (e.g. 6E10 and 4G8) (Fig.1). The preparations of Aß1-42 oligomers were not stained by 6E10 antibody (Fig.1), while samples of Aß1-42 oligomers stained by 4G8 antibody showed two reactive bands in the molecular weight range of a dimer-tetramer (10-20 kDa) conformation (Fig.1). Samples of Aß42-1 peptide were not stained by antibodies against Aß (Fig.1). In Aß1-42 oligomer-injected animals, immunoblotting with 6E10 antibody revealed the presence of a certain amount of high-molecular weight species at the injection site at an early (24h) step of Aß toxicity (Fig.1).

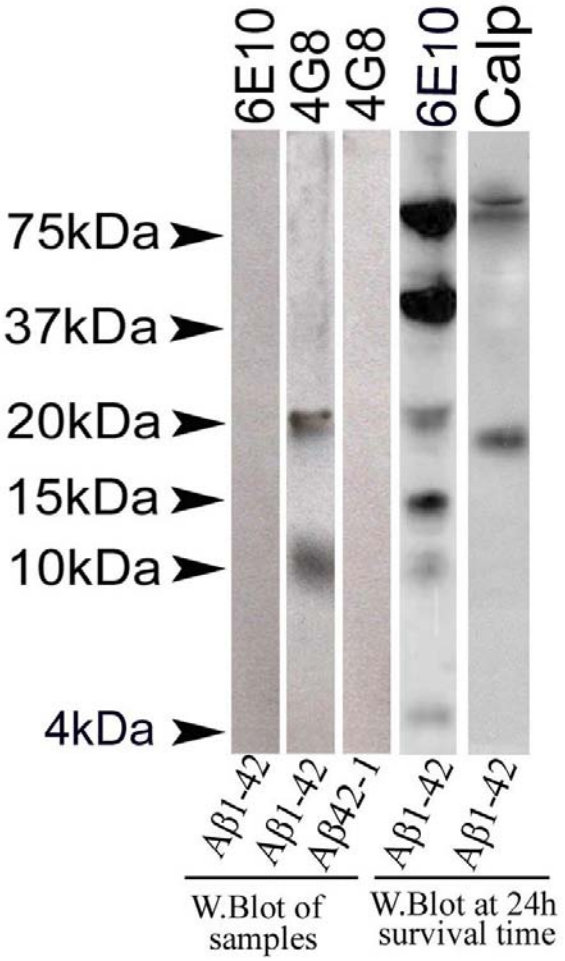

Figure 1. Synthetic Aß1-42 and Aß42-1 samples were run on 15% PAGE-SDS gels, transferred to nitrocellulose and incubated with 6E10 and 4G8 antibodies. Aß1-42 oligomers samples contain bands that react with 4G8 ranging from dimers to tetramers, while this sample does not stain with 6E10 antibody. Samples of control (Aß42-1) peptide do not stain with 4G8 antibody. Western blotting analyses of Aß peptide from rat brain extracts incubated with 6E10, following injections of Aß1-42 oligomers into the retrosplenial cortex, detected bands ranging from monomers-dimers-trimers-tetramers to large aggregates (75-80 kDa molecular weight), while Western blotting analysis of calpain-1 from rat brain extracts showing the proteolysis of three calpain-1 subunits, at approximately positions 80-kDa, 76-kDa, and 18-kDa.

Neuronal loss and synaptic alterations in Aß-injected animals

The findings reported here are based on all animals that received a single microinjection of Aß1-42 oligomers into the left retrosplenial cortex. As controls, a second group of animals received microinjections of Aß42-1 peptide into the corresponding regions of the left retrosplenial cortex. Immunocytochemical analysis revealed an intense Aß-immunoreactivity at the level of Aß1-42 injection site, particularly in the retrosplenial granular (RSg) and retrosplenial agranular (RSa) cortices at an early (24h) post-injection time (e.g., Fig.2A), and slight increases at later (72h) time points (e.g., Fig.2B). Control injection of Aß42-1 peptide showed a light background staining surrounding the injection site in the corresponding regions of the left retrosplenial cortex at all time point (e.g., Fig.2C).

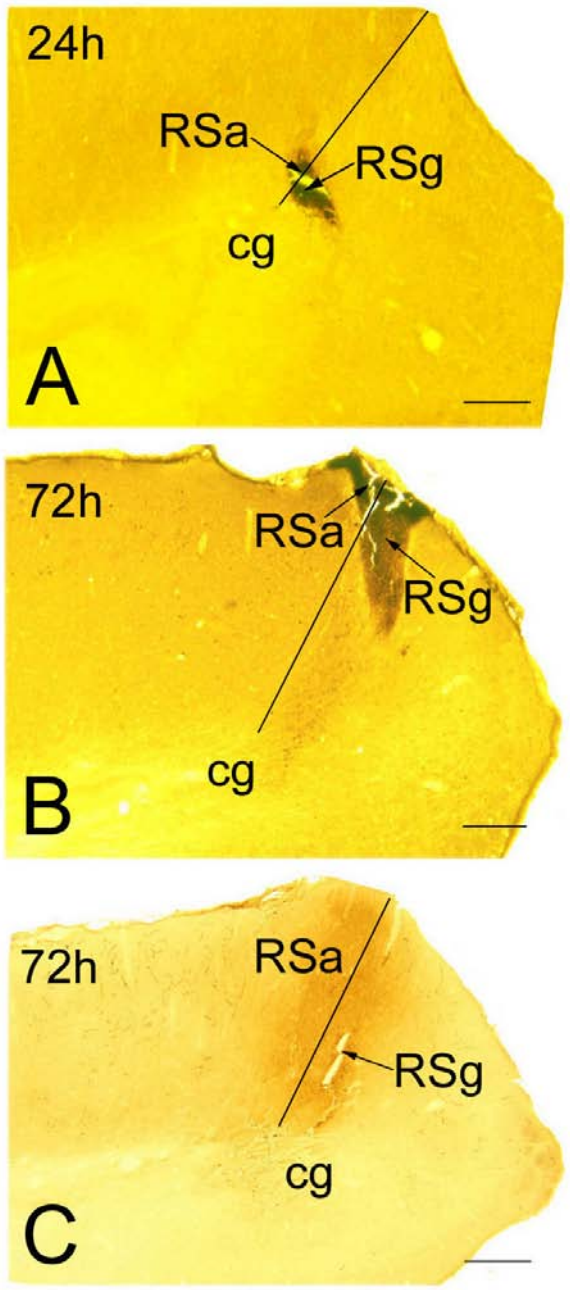

Figure 2. A-C. Photomicrographs of coronal sections through the retrosplenial cortex from sections subjected to Aß-immunohistochemistry (using 6E10 antibody) showing a dark staining at the level of representative injections of Aß1-42 into the left RSg, at 24h (A, arrow), and 72h (B, arrow) post-injection time, whereas a weak staining was observed at level of injection of Aß42-1 (control injection) at 72h post-injection time (C, arrow). Scale bars: 250µm (A-C).

Qualitative analysis of Nissl-stained sections revealed that all injections of Aß1-42 peptide (e.g., Fig. 3A) resulted in a marked reduction in the numbers of cresyl violet-stained cells as compared with those seen in the control (Aß42-1) injected animals (e.g., Fig. 3B). As reported previously (Gonzalo-Ruiz et al., 2006), the results of the qualitative analysis and quantitative measurements revealed considerable variance in the reduction of neurons between groups and according to the injection type (data don't shown). Brain sections from the Aß1-42 injected animals, stained with an antibody to NeuN, exhibited a marked decrease in NeuN-positive cells at the level of Aß1-42 injection site at early time points (e.g. Fig. 3C). We next examined whether neuronal loss in Aß1-42 injected animals occurred via apoptosis, which is associated with programmed cell death in response to highly selective cytotoxic agents. In paraffin-embedded tissue sections from the Aß1-42-injected animals, TUNEL assays were performed using the Oncor ApopTag peroxidase detection kit, which detects the 3'-OH region of cleaved DNA during apoptosis. In the Aß1-42 injected animals, the DNA Fragmentation Kit allowed the identification of a few apoptotic like-nuclei surrounding the injection site into the retrosplenial cortex at an early (24h) time point (e.g., Fig.3D). These findings suggested that Aß1-42 oligomers *in vivo* in the rat brain were triggering pathological cascades, leading to neuronal death at early stages of Aß toxicity, and that the retrosplenial cortex appears to be particularly vulnerable to toxic effects of Aß oligomers.

To examine synaptic alterations *in vivo*, brain sections from Aß oligomer-injected rats were stained with antibodies against synaptophysin and chromogranin A proteins. In Aß oligomer-injected animals we observed a marked decrease in synaptophysin immunoreactivity at the center of the injection of Aß peptide, whereas an increase in synaptophysin-immunopositive grains was observed

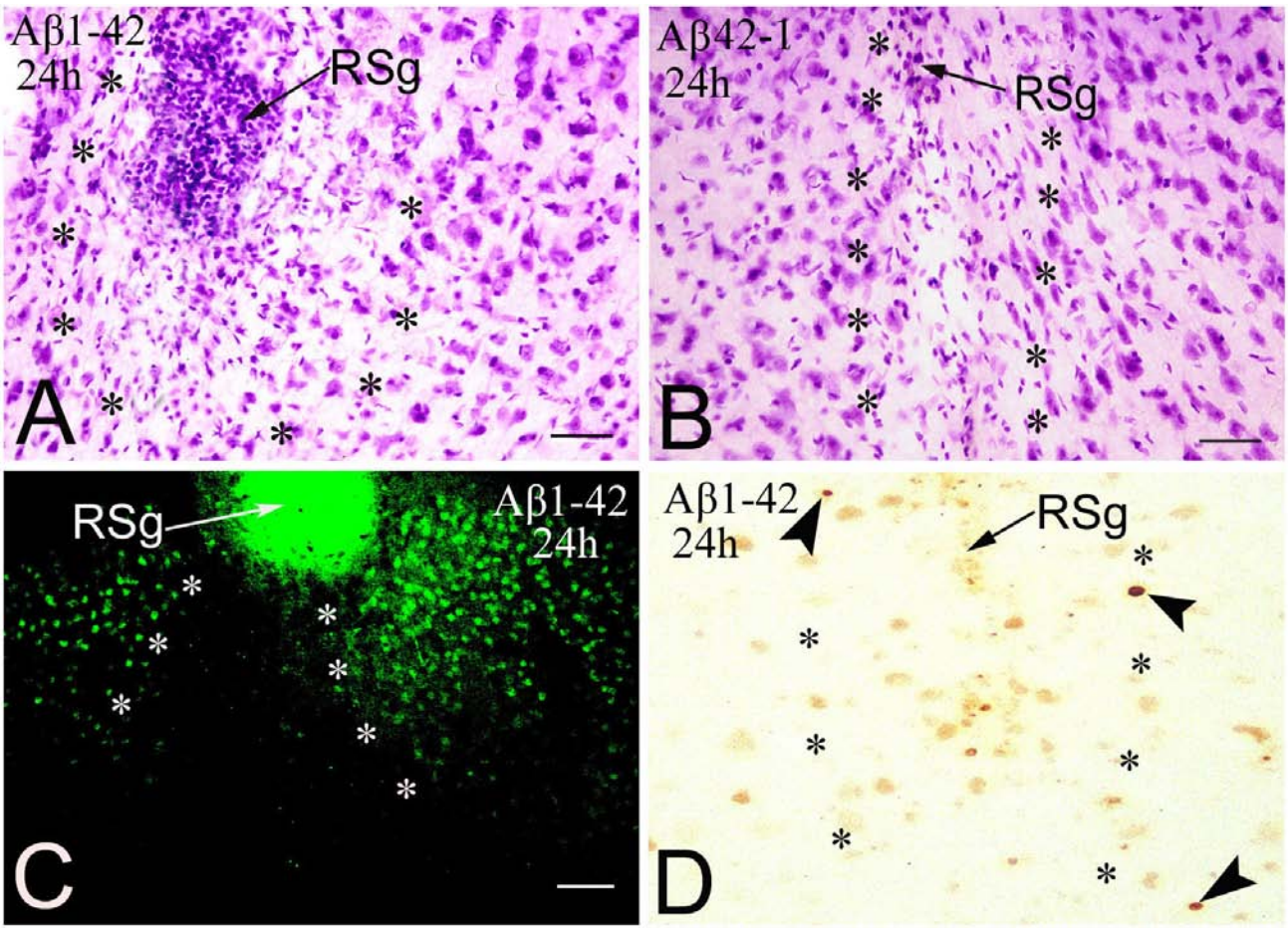

Figure 3. A, B. Cresyl violet-stained sections through the RSg following an injection of Aß1-42 oligomers (**A**), and a control (Aß42-1) injection (**B**). The area of the lesion and the reduction in cresyl violet-stained cells are considerably higher in Aß1-42 injected animals (A) as compared with controls (B). The field in (**C**) shows a marked decrease in NeuN-immunopositive cells at the injection of Aß oligomers into the RSg. Note also a few apoptotic like-nuclei in close association with the injection of Aß1-42 (**D,** arrowheads) at an early time point. Asterisks delineate the area of lesion induced by Aß peptide. Scale bars: 50 µm (A-D)

surrounding the deposit of Aß deposit at an early time point (Fig. 4A,B), increasing in an age-dependent fashion. Confocal image analysis of sections immunostained for co-localization of Aß and synaptophysin proteins revealed that all injections of Aß oligomers centred on the retrosplenial cortex (Fig.4C) resulted in Aß-, and synaptophysin-immunoreactive material surrounding the injection site of Aß (Fig.4C,D). Aß- and synaptophysin-immunopositive material co-localized in small granules associated with presynaptic vesicle protein (Fig. 4E). Brain sections from Aß oligomer-injected animals stained with antibody against chromogranin A showed a marked increase in chromogranin A-immunoreactivity at the centre of the injection of Aß peptide at early (24h-72h) time points (Fig. 4F,G). Confocal image analysis of sections immunostained for the co-localization of Aß and chromogranin A proteins revealed a marked increase in chromogranin A-immunoreactivity that infiltrated the injection site of Aß peptide (Fig. 4H). Immunoreactivity for Aß was also observed at the center of the injection site (Fig. 4I), and Aß- and chromogranin A-immunopositive material co-localized in small granules, particularly at the centre of the injection of Aß peptide (Fig. 4J).

Aß-immunopositive material in reactive astrocytes *in vivo* in the rat brain

In keeping with our earlier results (Perez et al., 2010), confocal image analysis of sections immunostained for the co-localization of Aß and GFAP proteins, revealed that all injections of Aß1-42 oligomers centred on the retrosplenial cortex (e.g., Fig. 5A) resulted in reactive astrocytes (e.g., Fig.5B), and in an intense accumulation of Aß-immunopositive material in astrocytes that surrounded and infiltrated the injection of Aß (e.g., Fig. 5C). In Aß oligomer-injected animals, immunoreactivity for Aß was also highly localized within the cytoplasm and in an elaborate network of reactive astrocytes that surrounded blood vessel at the early time point

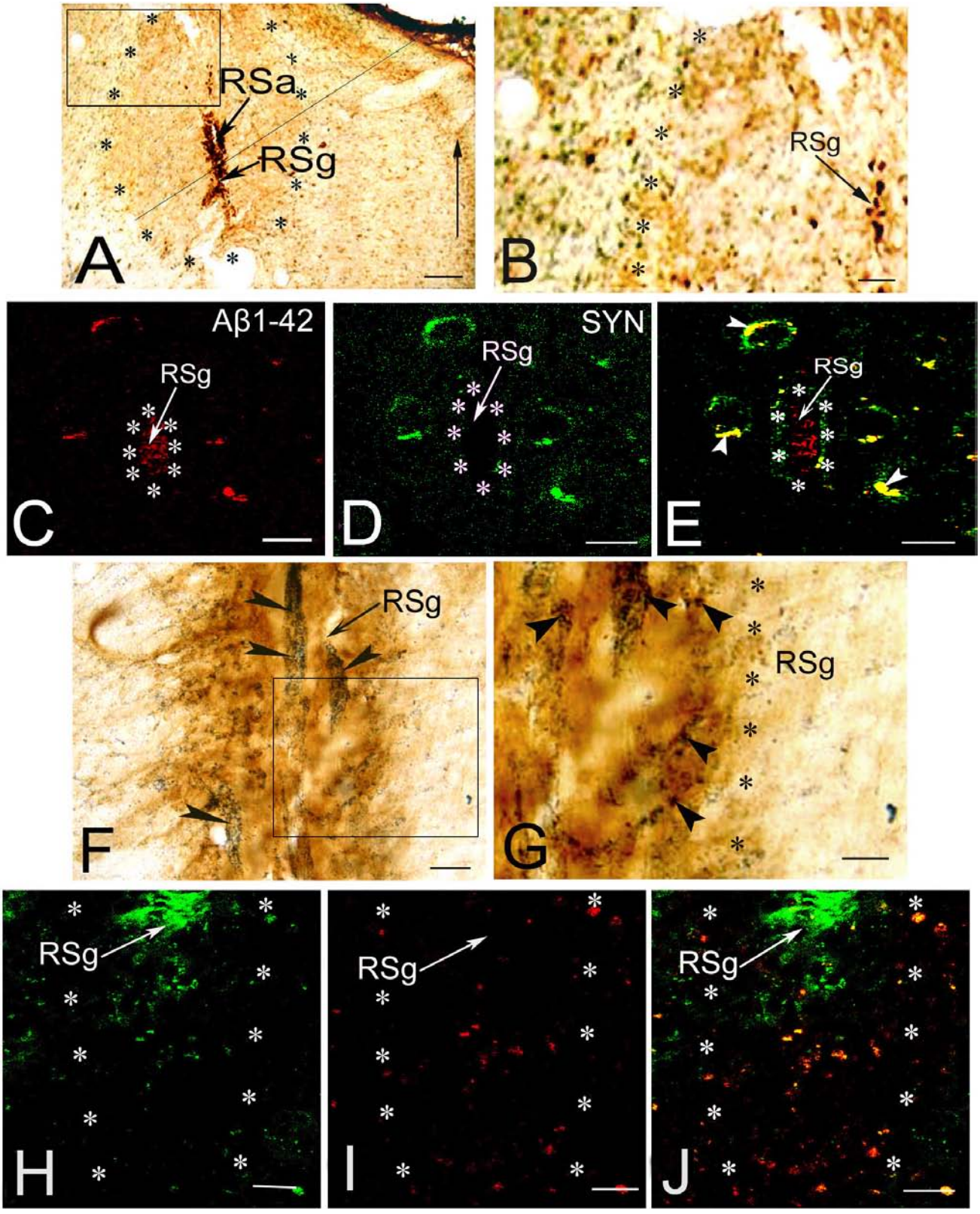

Figure 4. A, B. Photomicrographs of coronal sections through the RSg following an injection of Aß1-42 oligomers into the left RSg (arrows). Asterisks delineate the Aß-injected site. The straight arrow indicates the midline. The sections processed for co-localization of Aß peptide (DAB) and synaptophysin (using BDHC) show a dark brown staining for Aß and weak immunoreactivity for synaptophysin at the centre of the injection site (**A**), while an increase in synaptophysin-immunopositive material is seen at the periphery of Aß-injected site (**B**, dark-blue granules). **C-E.** Confocal images of the left RSg processed for co-localization of Aß peptide (using rhodamine, **C**) and synaptophysin (using FITC, **D**), following an injection of Aß1-42 oligomers into the left RSg (C, D, arrows). The field in **E** shows synaptophysin-immunopositive granules co-labelled with Aß peptide (yellow, arrowheads) surrounding the center of the Aß-injected site (red, delimitated by asterisks). **F.** Photomicrograph of coronal sections through the RSg following the injection of Aß1-42 oligomers into the left RSg (arrow). The section processed for co-localization of Aß peptide (DAB) and chromogranin A (using BDHC), shows a dark brown staining for Aß and a marked immunoreactivity for chromogranin A at the centre of the injection site (dark blue, arrowheads). The boxed area is enlarged in (G) **G.** Higher magnification of part of Fig. 4F, showing a marked increase in chromogranin A-IR (dark blue, arrowheads) at the centre of the Aß deposit (brown). Asterisks delineate the Aß-injected site. **H-J.** Confocal image of the left RSg processed for co-localization of chromogranin A (using FITC, **H**), and Aß peptide (using rhodamine, **I**). The field in **J** shows chromogranin A-immunopositive grains co-labelling with Aß-immunopositive material at the centre of the Aß-injected site (yellow). Scale bars: 250 µm (A), 100µm (C-F), 50µm (B, G-J).

of Aß toxicity (e.g., Fig. 5D, E). Confocal image analysis also revealed prominent granules of Aß-immunopositive material infiltrating the endothelial blood vessels (e.g., Fig. 5E). In addition, intense Aß-immunopositive material was observed in the cytoplasm and in astrocyte processes of reactive astrocytes, extending along the subventricular zone of the lateral ventricle, ipsilateral and contralateral to the injection of Aß (e.g., Fig. 5F).

Oligomers of Aß1-42 increase the activity of calpain-1 in rat brain

Western blotting analysis of the retrosplenial cortex from Aß1-42-treated animals and from control (Aß42-1) animals showed that the anti-calpain-1 antibody yielded a pattern of three immunopositive bands located at the large calpain-1 subunit (80 kDa), approximately at its 76 kDa fragment, and at 18 kDa molecular weight (Figs. 6A, 7A). The results

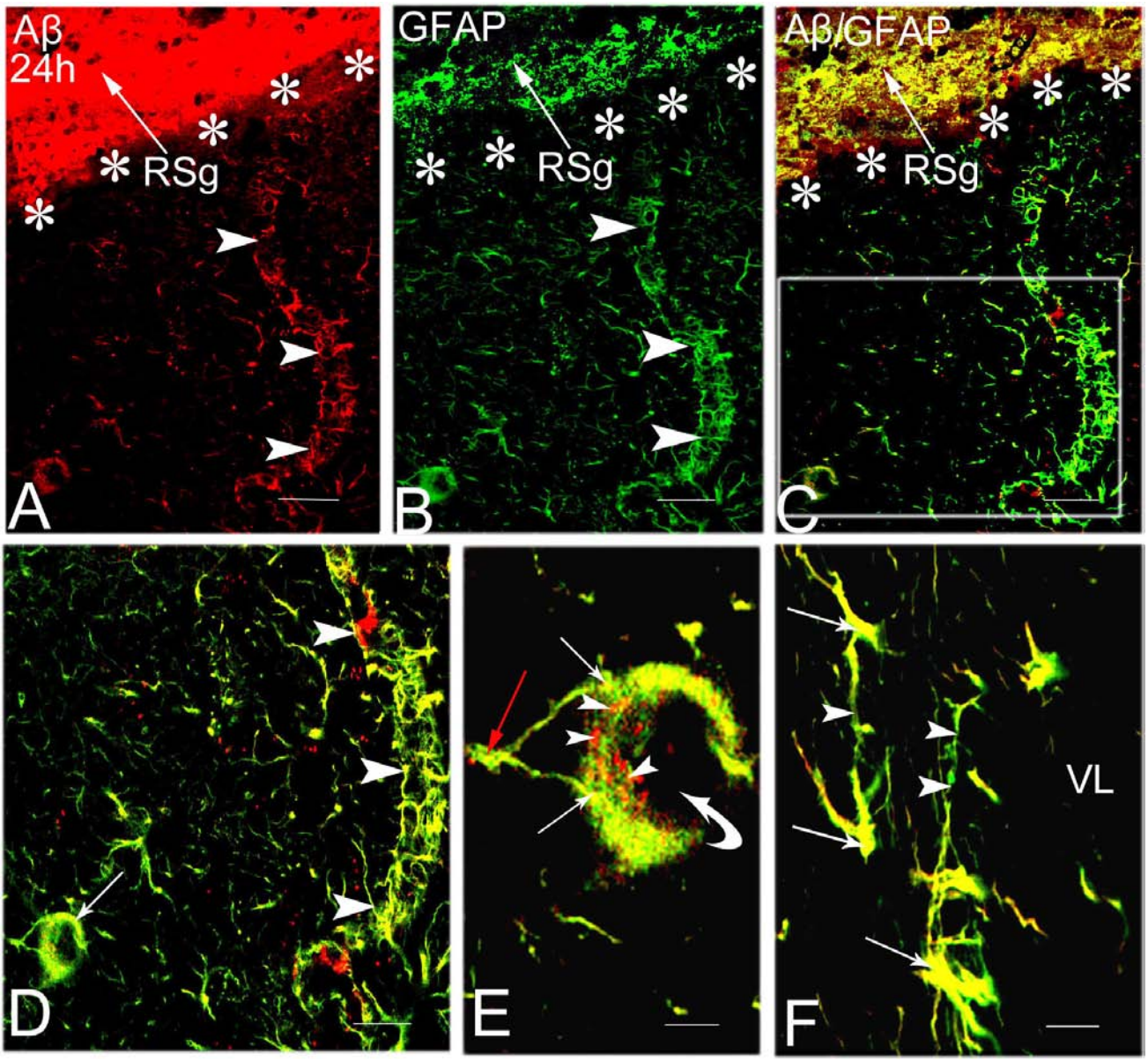

Figure 5. A-C. Confocal images of a coronal section through the RSg following an injection of Aß oligomers into the left RSg, at an early (24h) time point. The section was processed for the co-localization of Aß peptide (using rhodamine) and GFAP (using FITC). The field in (**A**) shows Aß-immunoreactivity at the level of the Aß-injected site (red, large arrow). The area of Aß-immunoreactivity is delineated by asterisks. Note also Aß-immunopositive material surrounding a blood vessel (arrowheads). The field in (**B**) shows reactive astrocytes (green), that surround the Aß-injected site (large arrow), delineated by asterisks, and a blood vessel (arrowheads). The field in (**C**) shows co-labelling of both proteins (Aß/GFAP, yellow) surrounding and infiltrating the injection site (arrow) marked by asterisks. The boxed area is enlarged in (D). **D.** Co-labelling for Aß and GFAP-immunoreactivity surrounding and infiltrating a blood vessel (arrowheads). The blood vessel indicated with an arrow is enlarged in (E). **E.** Higher magnification of a blood vessel (curved arrow) showing Aß-immunopositive material infiltrating the endothelial blood vessel (red, arrowheads). Note also a double-labelled astrocyte (red arrow) and astrocyte processes in close association with the endothelial blood vessel (arrows). **F.** Double-labelled astrocytes (yellow, arrows), and astrocyte processes (arrowheads) extend along the subventricular zone of the lateral ventricle. Scale bars: 75µm (A-C), 50µm (D), 25µm (F), 10µm (E).

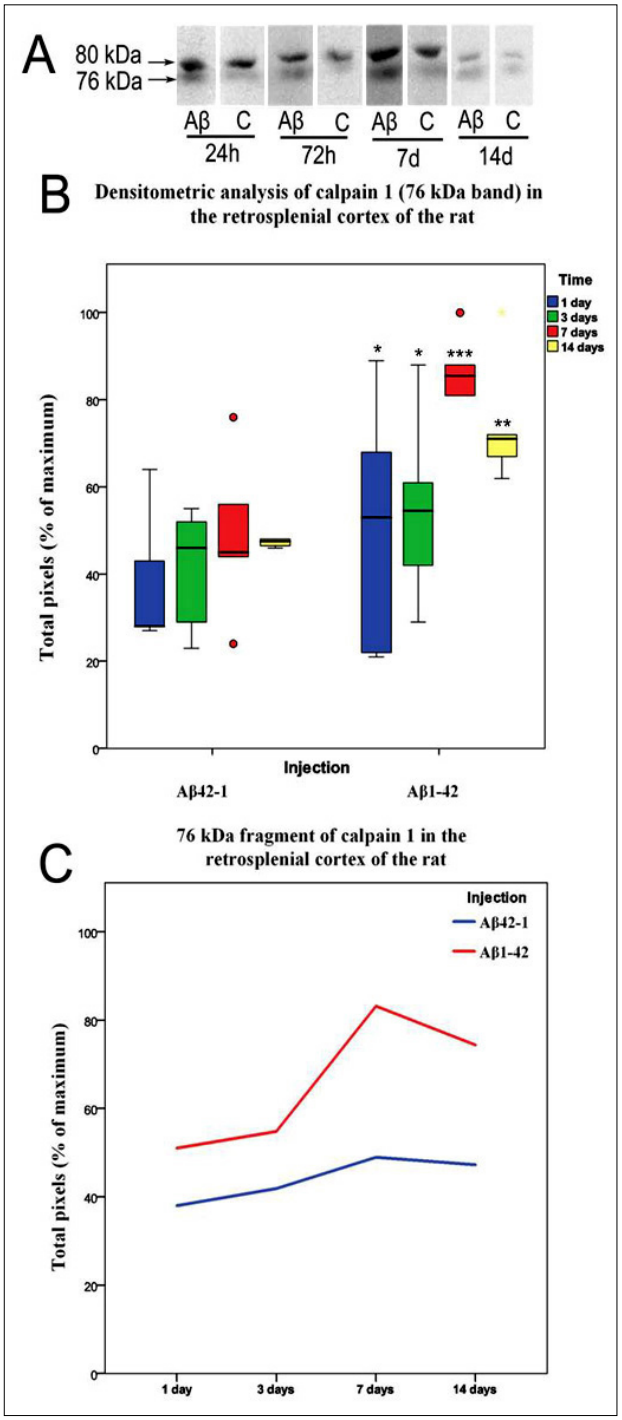

Figure 6. A. Representative pattern of calpain-1 protease bands at positions 80 kDa and 76 kDa, corresponding to Aß1-42 (Aß)- or Aß42-1 (control, C)-treated rats, following 24h, 72h, 7d, and 14d after treatment. **B.** Densitometric analysis of a 76 kDa band in the retrosplenial cortex following injections of either Aß1-42 peptide or Aß42-1 (control animals) in the different situations tested. **C.** Time-course graph of active calpain-1 at its 76 kDa fragment in Aß1-42- or Aß42-1-treated rats (mean values). In B and C, the data correspond to values obtained in at least three experiments for each situation tested (four rats per group). Statistical differences among groups were calculated by means of Student's *t*-test if normal distribution could be assumed or with the non-parametric Mann-Whitney U-test if normality was not valid. *p < 0.5, **p < 0.05, ***p < 0.01, Aß1-42-treated rats *versus* Aß42-1 animals (control rats)

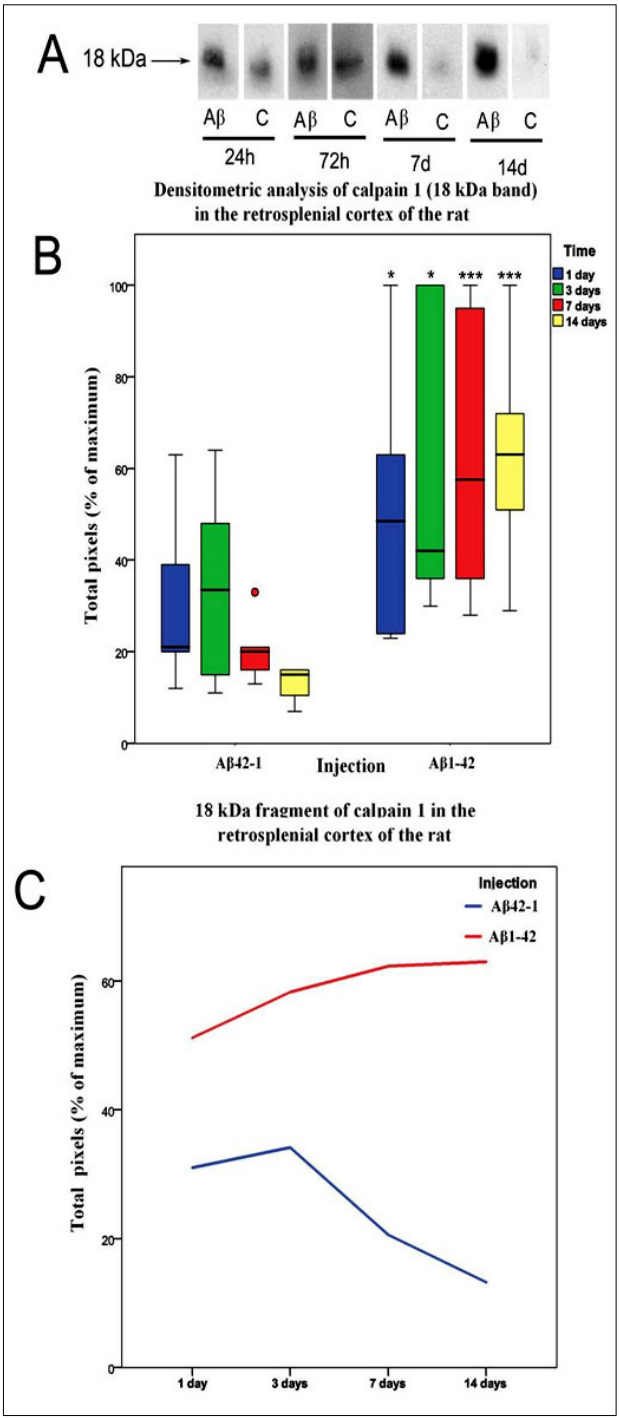

Figure 7. A. Representative pattern of immunoblot detection of active calpain-1 at position 18 kDa from Aß1-42 (Aß)- or Aß1-42 (control, C)-treated rats, at 24h, 72h, 7d, and 14d after treatment. **B.** Densitometric analysis of the 18 kDa fragment in the retrosplenial cortex after injections of either Aß1-42 or Aß42-1 (control animals) in the different situations tested. **C.** Time-course graph of active calpain-1 at position 18 kDa in Aß1-42- or Aß42-treated rats (mean values). In B and C, the data correspond to the values obtained in at least three experiments for each situation tested (four rats per group). Statistical differences among groups were calculated by means of Student's *t*-test if normal distribution could be assumed or with the non-parametric Mann-Whitney U-test if normality was not valid. *p < 0.5, ***p < 0.01, Aß1-42-treated rats *versus* Aß42-1 (control rats)

of the densitometry analysis revealed significant differences in the levels of active calpain-1 at the 76 and 18 kDa positions by injection type and by survival time (Figs. 1E, 6A-C, 7A-C). Thus, in Aß1-42 oligomer-treated animals we found statistically significant increases of 41% ($p < 0.01$, Mann-Whitney U-test) and of 36.49% ($p < 0.05$, Mann-Whitney U-test) in the density of a 76kDa band after 7d and 14d, respectively, as compared with that seen in the corresponding band in the control (Aß42-1) animals at the same time points (Table 1A, Fig. 6B,C). In oligomer-treated animals, there was also a significant increase of 38.63%, and of 31.35% in the density of the band at the 76 kDa position at 7d and 14d, respectively, as compared with the corresponding band at the earlier (24h) time point (Table 1B, Fig.6B, C). In the control animals, injections of Aß42-1 peptide into the retrosplenial cortex resulted in a non-statistically significant difference of 22.45% in the density of a 76 kDa band at 7d post-injection, as compared with that seen in the corresponding fragment of calpain-1 at the early time points (Table 1C, Fig. 6C).

In Aß1-42 oligomer-injected animals, immunoblot staining with anti-calpain 1 antibody also revealed statistically significant increases of 67% ($p < 0.01$, Mann-Whitney U-test), and of 79% ($p < 0.01$, Mann-Whitney U-test) in the density of a 18 kDa band after 7d and 14d, respectively, as compared with that seen in the corresponding band in control animals at the same time points (Table 2A, Fig. 7B, C). In Aß oligomer-treated animals, there was a non-statistically significant difference of 18%, and of 18.8% in the density of the band at the 18 kDa position at 7d and 14d, respectively, as compared with the corresponding band at the

Table 1. Quantitative analysis of the expression of a 76-kDa fragment of calcium-dependent protease calpain-1 following injections of Aß1-42 oligomers and of a reversible form of Aß1-42 peptide (control injection) into the left retrosplenial cortex.

Injection	Survival time	% of maximum total pixels (mean ± S.D)	95% Confidence interval of the difference	% Difference	*p* value
A		23^{a}			
Aß1-42	24h	51 ± 9.4	$16.05\text{-}29.95^{a}$	$25.49\%^{a}$	$<0.5^{a}$ (Mann-Whitney U)
		13^{b}			
	72h	54.83 ± 8.1	$5.84\text{-}20.16^{b}$	$23.7\%^{b}$	$<0.5^{b}$ (Mann-Whitney U)
		32.4^{c}			
	7d	83.17 ± 5.5	$41.73\text{-}23.1^{c}$	$41\%^{c}$	$<0.01^{c}$(Mann-Whitney U)
		27.1^{d}			
	14d	74.40 ± 6.6	$10.24\text{-}44^{d}$	$36.49\%^{d}$	$<0.05^{d}$(Mann-Whitney U)
Aß42-1	24h	38.00 ± 7.1			
	72h	41.83 ± 5.3			
	7d	49.00 ± 8.4			
	14d	47.25 ± 0.4			
B			6.16^{e}		
Aß1-42	24h	51 ± 9.4	$0.2\text{-}12.1^{e}$	$7\%^{e}$	0.589^{e} (Mann-Whitney U)
			22.16^{f}		
	72h	54.83 ± 8.1	$34.8\text{-}9.5^{f}$	$38.63\%^{f}$	$<0.5^{f}$ (Mann-Whitney U)
			13.35^{g}		
	7d	83.17 ± 5.5	$21.7\text{-}5.0^{g}$	$31.35\%^{g}$	$<0.5^{g}$ (Mann-Whitney U
	14d	74.40 ± 6.6			
C			6.17^{h}		
Aß42-1	24h	38.00 ± 7.1	$2.34\text{-}10^{h}$	$9.16\%^{h}$	0.537^{h} (Mann-Whitney U)
			12.6^{i}		
	72h	41.83 ± 5.3	$9.12\text{-}16.15^{i}$	$22.45\%^{i}$	0.421^{i} (Mann-Whitney U)
			18.3^{j}		
	7d	49.00 ± 8.4	$9.0\text{-}27.61^{j}$	$19.58\%^{j}$	0.190^{j} (Mann-Whitney U)
	14d	47.25 ± 0.4			

The density of a 76-kDa fragment of calcium-dependent protease calpain-1 in the retrosplenial cortex was analyzed as described in Material and Methods.

(a-d) Differences in the density of a 76-kDa fragment of calpain-1 between Aß1-42 injected animals and control (Aß42-1) animals following 24h (**a**), 72h (**b**), 7days (**c**), and 14 days (**d**), survival time.

(e-g) Differences in the density of active calpain-1, at 76-kDa molecular weight, between 24h and 72h (**e**), 24h and 7 days (**f**), 24h and 14 days (**g**), after injections of Aß1-42 oligomers.

(h-j) Differences in the density of a 76-kDa fragment of calpain-1between the first 24h and 72h (**e**), 24h and 7 days (**f**), and 24h and 14 days (**g**), following injections of Aß42-1 peptide.

earlier (24h) time point (Table 2B, Fig. 7B,C). By contrast, in control animals, the 18 kDa band of active calpain-1 showed a maximum density at 72h post-injection time, after which the intensity of this band yield a statistically significant decrease of 33.5%, and of 57.26% at 7d and 14d, respectively, as compared with the earlier (24h) survival time (Table 2C, Fig. 7B, C).

In conclusion, immunoblot staining with anti-calpain 1 revealed that the most extensive increase in the density of the bands at approximately 76 and at 18 kDa molecular weight occurs at 7d and 14d after the injection of Aß1-42 oligomers into the retrosplenial cortex.

Colocalization of Aß-immunopositive material and calpain 1-immunoreactivity in the rat brain

Double-labelling immunohistochemical studies for Aß and calpain-1 revealed that injections of Aß1-42 oligomers centred on the retrosplenial cortex resulted in an intense colocalization of both proteins which surrounded and infiltrated the entire rostro-caudal extent of the injection of Aß (e.g., Fig. 8A). The central region of the Aß injection showed a dense amorphous calpain 1-immunopositive material, whereas the periphery of the injection had large numbers of calpain 1-immunoreactive cell bodies (e.g., Fig. 8A, B). In the Aß oligomer-injected animals, immunoreactivity for calpain-1 was also local-

Table 2. Quantitative analysis of the expression of a 18-kDa fragment of calcium-dependent protease calpain-1 following injections of Aß1-42 oligomers and of a reversible form of Aß1-42 peptide (control injection) into the left retrosplenial cortex.

Injection	Survival time	% of maximum total pixels (mean ± S.D)	95% Confidence interval of the difference	% Difference	*p* value
A		20.18^{a}			
Aß1-42	24h	51.2 ± 6.5 20.6^{b}	$15.6\text{-}24.7^{a}$	$35.4\%^{a}$	$<0.5^{a}$ (Mann-Whitney U)
	72h	58.3 ± 3.4 23.1^{c}	$4.0\text{-}37.2^{b}$	$41.4\%^{b}$	$<0.5^{b}$ (Mann-Whitney U)
	7d	62.3 ± 9.8 34.5^{d}	$16.0\text{-}30.2^{c}$	$67\%^{c}$	$<0.01^{c}$ (Mann-Whitney U)
	14d	63.0 ± 7.3	$23.5\text{-}45.5^{d}$	$79\%^{d}$	$<0.01^{d}$ (Mann-Whitney U)
Aß42-1	24h	31.0 ± 9.1			
	72h	34.1 ± 8.2			
	7d	20.6 ± 3.4			
	14d	13.2 ± 2.1			
B		7.2^{e}			
Aß1-42	24h	51.2 ± 6.5 11.1^{f}	$2.7\text{-}11.6^{e}$	$12{,}8\%^{e}$	0.818^{e} (Mann-Whitney U)
	72h	58.3 ± 3.4 11.3^{g}	$9.8\text{-}12.4^{f}$	$18\%^{f}$	0.485^{f} (Mann-Whitney U)
	7d	62.3 ± 9.8	$8.8\text{-}13.9^{g}$	$18.8\%^{g}$	0.329^{g} (Mann-Whitney U)
	14d	63.0 ± 7.3			
C		7.5^{h}			
Aß42-1	24h	31.0 ± 9.1 16.2^{i}	$0.8\text{-}14.2^{h}$	$9.1\%^{h}$	0.429^{h} (Mann-Whitney U)
	72h	34.1 ± 8.2 18.5^{j}	$9.4\text{-}23.0^{i}$	$-33.5\%^{i}$	0.792^{i} (Mann-Whitney U)
	7d	20.6 ± 3.4	$0.85\text{-}36.2^{j}$	$-57.2\%^{j}$	$<0.5^{j}$ (Mann-Whitney U)
	14d	13.2 ± 2.1			

The density of an 18-kDa fragment of calcium-dependent protease calpain-1 in the retrosplenial cortex was analyzed as described in Material and methods.

(a-d) Differences in the density of an 18-kDa fragment of active calpain-1 between Aß1-42 injected animals and control (Aß42-1) animals after 24h (**a**), 72h (**b**), 7days (**c**), and 14 days (**d**), survival time.

(e-g) Differences in the density of calpain-1 at 18-kDa molecular weight between 24h and 72h (**e**), 24h and 7 days (**f**), and 24h and 14 days (**g**), following injections of Aß1-42 peptide.

(h-j) Differences in the density of calpain-1 at 18-kDa molecular weight between 24h and 72h (**e**), 24h and 7 days (**f**), and 24h and 14 days (**g**), following injection of Aß42-1 peptide.

ized in structures-like diffuse aggregates forms, showing profiles with features of filaments in several cortical regions, such as in the frontal, and temporal cortices, ipsilateral and contralateral to the Aß-injected site (e.g., Fig. 8C). In Aß-immunopositive aggregate forms, calpain 1-immunoreactive material was most commonly localized in prominent granules distributed without a defined outline (e.g., Fig. 8C). Control injections of Aß42-1 peptide, by contrast, showed a rather homogenous and weak calpain-1 staining at the injection site (e.g., Fig. 8D). In Aß oligomer-injected animals, in addition to the pattern of labelling described above Aß-, and calpain 1-immunopositive material was observed in cortical cells (e.g., Fig. 8E, F,H,I), which displayed a triangular soma and had large apical

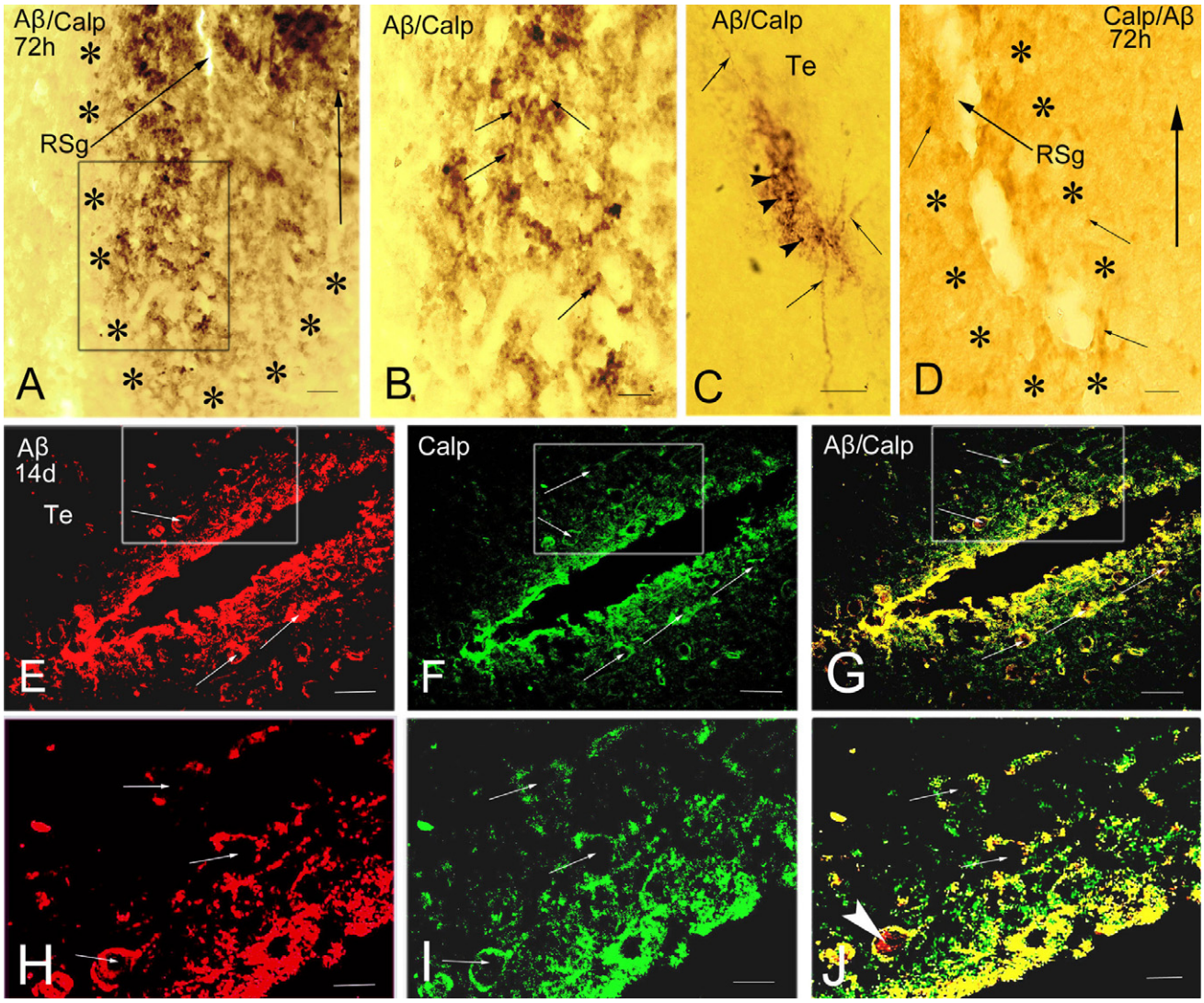

Figure 8. A. Photomicrograph of coronal sections through the RSg following an injection of Aß1-42 oligomers into the left RSg (arrow). Asterisks delineated part of the Aß-injected site. The straight arrow indicates midline. The sections processed for co-localization of Aß peptide (using DAB) and calpain-1 protease (using BDHC) show co-labelling of both proteins (Aß/calpain-1) at the centre (dark brown area) and at the periphery of Aß-injected site (e.g., labelling marked by a rectangle). **B.** High magnification of the boxed area in (A), showing double-labelled (Aß/calpain-1) cell bodies (arrows). **C.** Calpain 1-immunopositive material (arrowheads) accumulates in Aß-immunoreactive aggregate form with apparently diffuse filaments (arrows) in the temporal cortex. **D.** Representative example of sections processed for the co-localization of calpain-1 (using DAB) and Aß peptide (using BDHC), after an injection of Aß42-1 (control injection) into the left RSg (large arrow). Asterisks mark part of the injection site. The straight arrow indicates the midline. The field shows slightly calpain-1 immunoreactive cell bodies at the injection of Aß42-1 peptide (brown, small arrows). **E-G.** Confocal images of coronal sections through the temporal cortex of the rat brain processed for co-localization of Aß peptide (using rhodamine) and calpain-1 (using FITC) following an injection of Aß oligomers into the left RSg at 14 days survival time. The field in (E) shows Aß-immunoreactivity surrounding a blood vessel (red). Note also Aß-immunopositive material in cortical cells (arrows). The field in (F) shows calpain 1-immunoreactivity in cortical cells surrounding and infiltrating endothelial blood vessel (arrows). The field in (G) shows co-labelling for Aß and calpain 1-immunoreactivity, surrounding a blood vessel (yellow) and in cortical cell bodies (arrows). The boxed areas in (E), (F), and (G) are enlarged in (H), (I), and (J), respectively. **H-J.** Higher magnification of boxed areas in (E), (F), and (G) showing cortical cells immunoreactive either for Aß (H, arrows) and calpain-1 (I, arrows), or co-labelling for both proteins (Aß/calpain-1) (J, arrows). Note that the immuno-labelling is localized in cortical cells, which have a triangular shaped soma, and large apical process arising from the apex of the cell bodies (H-J, arrows). The field in (J) also shows Aß-immunopositive material accumulated in the cytoplasm of a cortical cell (red, arrowhead), which apparently exhibits co-localization of Aß- and calpain 1-immunoreactivity in the plasma membrane (yellow). Scale bars: 75 µm (A), 50 µm (B, D-G), 25 µm (H-J), 10 µm (C).

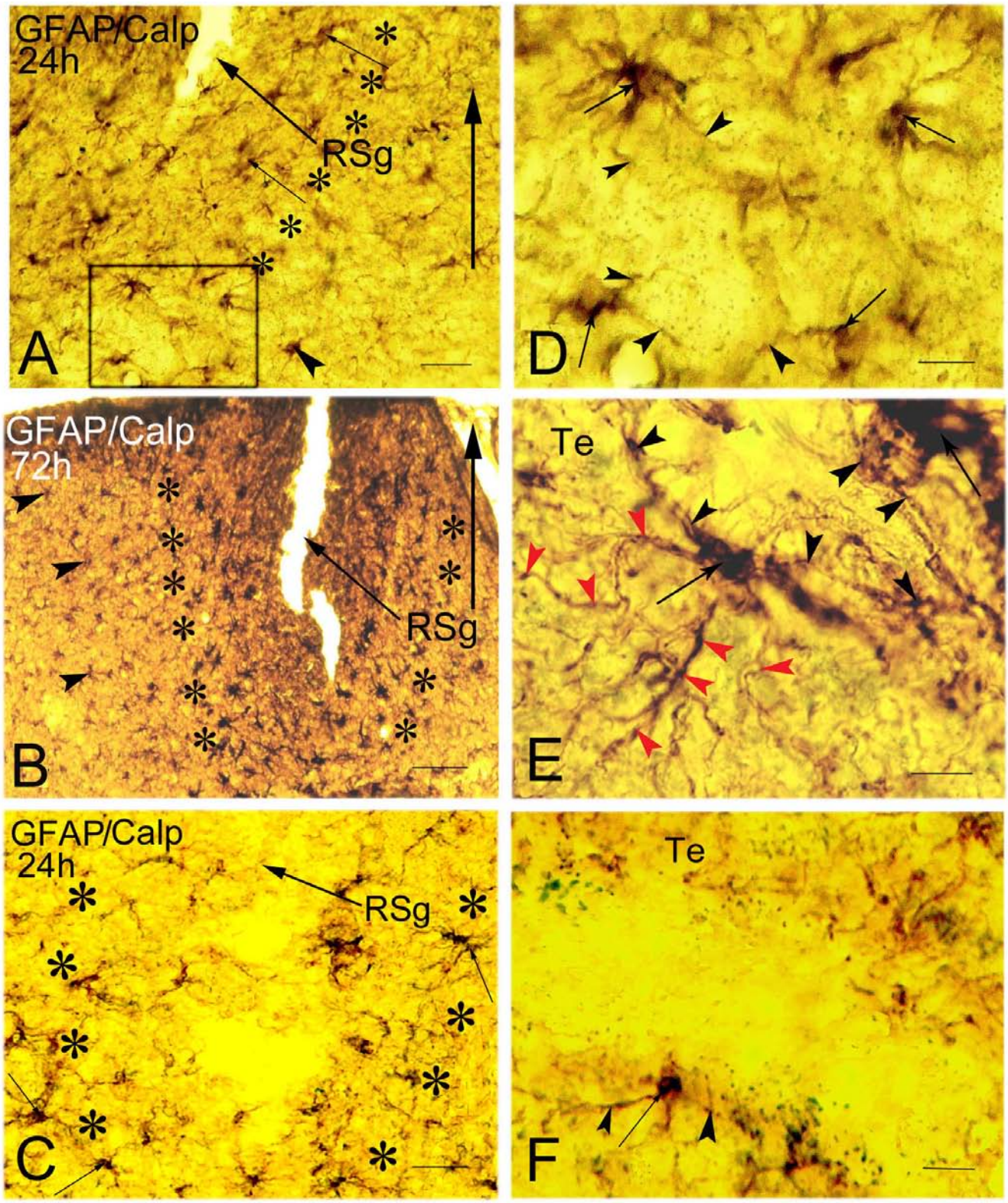

Figure 9. A, B. Photomicrographs of coronal sections through the retrosplenial cortex following injections of Aß1-42 oligomers into the left RSg cortex at early (24h) (A, large arrow) and later (72h) (B, large arrow) time points. Asterisks delineated part of the Aß-injected site. The sections processed for the co-localization of GFAP (using DAB) and calpain-1 (using BDHC) show double-labelled astrocytes surrounding (arrowheads) and infiltrating (small arrows) the injection site. The straight arrows in (A) and (B), indicate the midline. The boxed area in (A) is enlarged in (D). **C.** Photomicrograph of coronal section through the RSg after a control injection of Aß42-1 peptide into the left RSg (large arrow). The area of lesion is marked by asterisks. The section processed for co-localization of GFAP and calpain-1 immunohistochemistry shows few GFAP-immunoreactive cells surrounding the injection site (small arrows). **D.** High magnification of the boxed area in (A), showing co-labelling for GFAP and calpain 1-immunoreactivity in astrocyte cell bodies (arrows) and astrocyte processes (arrowheads) surrounding a blood vessel. **E.** Representative example of a section through the right temporal cortex after the injection of Aß oligomers shown in (B). The section processed for the co-localization of GFAP and calpain-1 shows double-labelled reactive astrocytes around a blood vessel (arrows). Note also calpain-1-immunopositive material in the astrocyte processes that surround a blood vessel (black arrowheads) and extend further to adjacent cortical tissue (red arrowheads). **F.** Photomicrograph of a coronal section through the temporal cortex following the injection of Aß42-1 peptide shown in (C). The section processed for co-localization of GFAP and calpain-1 shows a double-labelled astrocyte (arrow) and astrocyte processes (arrowheads), surrounding a blood vessel. Scale bars: 100 µm (B), 50 µm (A, C, F), 25 µm (D), 20 µm (E).

process arising from the apex of the cell's somata (e.g., Fig. 8H, I). Confocal images also revealed the co-localization of proteins (Aß and calpain-1), surrounding and infiltrating the endothelial blood vessels (e.g., Fig.8G, J).

Calpain 1- immunoreactivity in reactive astrocytes in the rat brain

Double-labelling (GFAP/calpain-1) immunohistochemical studies revealed that all injections of Aß1-42 oligomers centred on the retrosplenial cortex resulted in dense calpain 1-immunoreactivity in GFAP-positive cells, which surrounded and infiltrated the injection site of Aß at an early (24h) time point of Aß toxicity (Fig. 9A), increasing at a later (72h) stage (Fig. 9B). As shown in Figure 9B, calpain 1-immunopositive material in reactive astrocytes at the injection site of Aß oligomers can be divided into a area closer to the centre of the injection site and a peripheral region. The closest region contained large numbers of GFAP-positive cell bodies densely labelled for calpain-1 (Fig. 9B), while the periphery of the injection site had boured smaller numbers of calpain 1-immunopositive astrocytic cell bodies (Fig.9B). In the control animals, the injection of Aß42-1 peptide resulted in a weak calpain immunoreactivity in GFAP-positive cells surrounding the injection site at an early (24h) time point (Fig. 9C). In addition, calpain 1-immunopositive material was also observed in a population of reactive astrocytes and in a dense meshwork of astrocyte processes surrounding blood vessels in close association with the injection of Aß oligomers at the early time point (Fig. 9D), later (72h) increasing in blood vessels located some distance from the injection site, such as in the hippocampus and in several cortical regions (Fig.9E). In control animals, a weak calpain 1-labelling was also present in the cytoplasm and astrocyte processes surrounding blood vessels (Fig. 9F).

Double-labelling (GFAP/calpain-1) immunofluorescence studies confirmed that injections of Aß oligomers centred on the retrosplenial cortex resulted in large numbers of reactive astrocytes surrounding and infiltrating the injection of Aß (Fig.10A). Intensely stained calpain 1-immunopositive material was also observed in the cytoplasm and in astrocyte processes (Fig.10B). Confocal images analyzed showed a marked increase in calpain-1 immunoreactivity in GFAP-positive cell bodies and along astroyte processes at the injection of Aß oligomers (Fig. 10C). In addition to the pattern of co-labelling described above, dense calpain 1-immunopositive material was also observed in the cytoplasm and astrocyte processes of reactive astrocytes that surrounded cortical blood vessels after a survival time of 72h (Fig.10C), while a weak immunoreactivity for calpain-1 was present in astrocytes surrounding blood vessels at an early (24h) time point (Fig. 10D-F). GFAP-positive cells and a meshwork of astrocyte processes densely labelled for calpain-1 were also detected surrounding and infiltrating leptomeningeal blood vessels (Fig. 10G-I).

S100B-immunopositive material in reactive astrocytes in the rat brain

Double-labelling (GFAP/S100B) immunofluorescence studies confirmed that injections of Aß1-42 oligomers centred on the retrosplenial cortex resulted in large numbers of reactive astrocytes surrounding the injection of Aß1-42 peptide (Fig.11A). Intense S100B-immunopositive material was also observed in the cytoplasm and in astrocyte processes that surrounded the injection site (Fig. 11B). The confocal images analyzed revealed that all injections of Aß1-42 oligomers centred on the retrosplenial cortex resulted in an intense accumulation of S100B-immunopositive material in reactive astrocytes at the injection of Aß at 72h time point (Fig. 11C). In Aß oligomer-injected animals, GFAP-positive astrocytes and S100B-immunoreactivity was also observed extending further away from the site of amyloid injection to several cortical regions, such as the temporal cortex (Fig.11D-F), and hippocampus (Fig. 11G-I). In addition, S100B-immunopositive material also infiltrated and dominated the cytoplasm and astrocyte processes of activated astrocytes that surrounded blood vessels after 72h survival time (Fig.11F), while a weak immunoreactivity for S100B was present in astrocytes surrounding blood vessels at an early (24h) time point (Fig. 11J-L). In the control (Aß42-1) animals, a weak S100B-immunoreactivity was observed in GFAP-positive astrocytes in association with the injection site (data not shown).

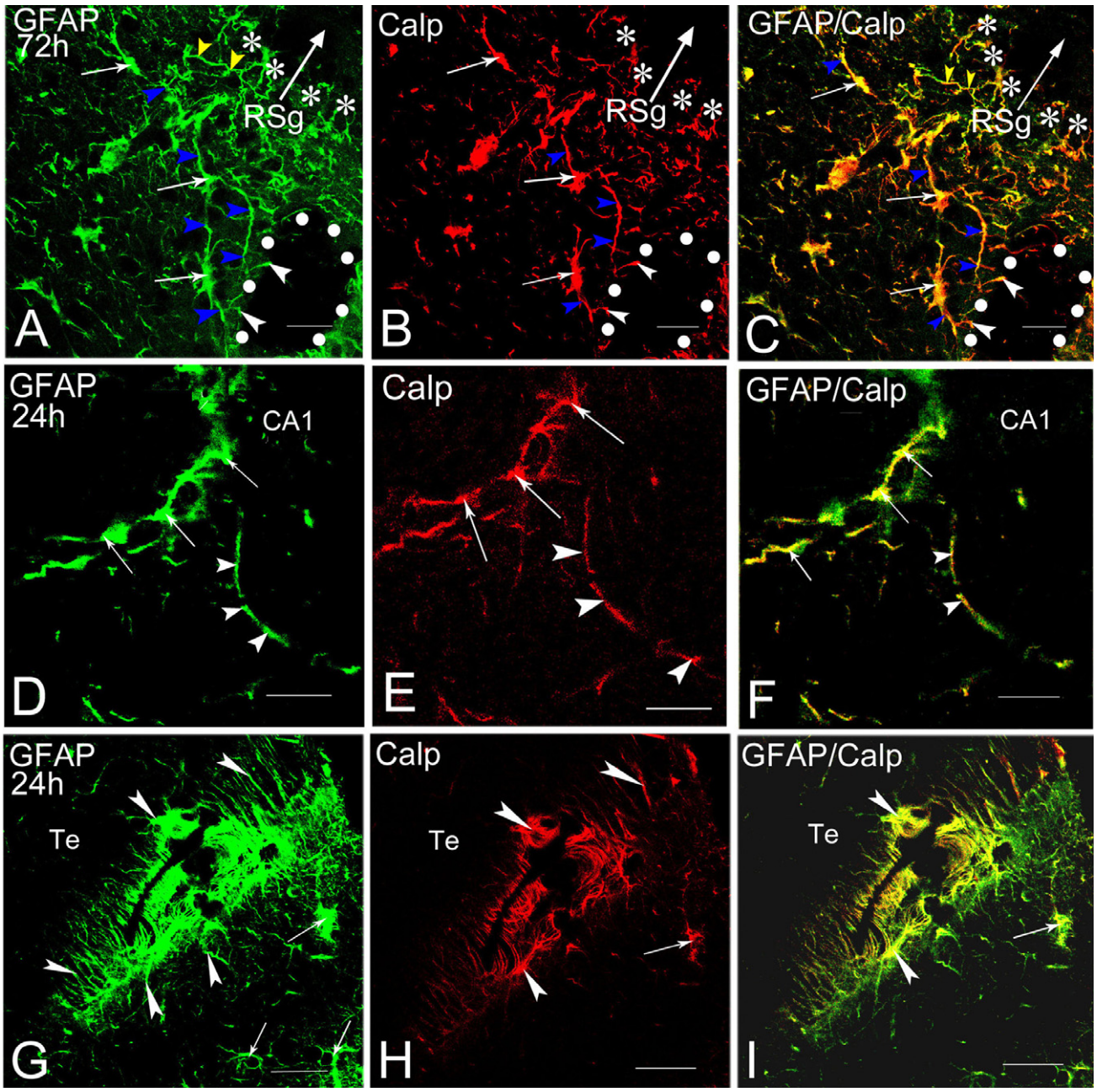

Figure 10. A-C. Confocal images of a coronal section through the RSg, after the injection of Aß oligomers into the left RSg, at 72h time point. The section was processed for the co-localization of GFAP (using FITC) and calpain-1 (using rhodamine). The field in (A) shows GFAP-immunoreactivity in the cytoplasm of reactive astrocytes (small arrows) and in astrocyte processes (yellow arrowheads) surrounding the Aß-injected site (large arrow), marked by asterisks. Note also astrocyte processes in contact with a blood vessel (white arrowheads), marked by spots and extending from the blood vessels to, and among, astrocytes (blue arrowheads). The field in (B) shows calpain 1-immunoreactivity in astrocytes (small arrows) around the area of lesion (large arrow), marked by asterisks. Note also immunoreactivity for calpain 1 in astrocyte processes in contact with a blood vessel (white arrowheads), delineated by spots, and extending between astrocytes (blue arrowheads). The field in (C) shows double-labelled astrocytes (yellow, small arrows) surrounding the Aß-injected site (large arrow), marked by asterisks. Note also that calpain 1-immunopositive material accumulates in the astrocyte processes (yellow) surrounding the injection site (yellow arrowheads) and extending from the blood vessel (white arrowheads), marked by spots, to and among reactive astrocytes (blue arrowheads). **D-I.** Representative example of sections through the hippocampus (D-F) and temporal cortex (G-I) processed for the co-localization of GFAP (using FITC) and calpain-1(using rhodamine) following an injection of Aß oligomers into the left RSg at early (24h) time point. **D-F.** Cofocal images of a coronal section through the ipsilateral CA1 of the hippocampus showing GFAP-immunoreactivity in the cytoplasm of reactive astrocytes (D, arrows) and in astrocyte processes (D, arrowheads), surrounding and infiltrating a blood vessel. The field in (E) shows calpain 1-immunopositive material accumulated around a blood vessel (arrows), and in astrocyte processes (arrowheads). The field in (F) shows double-labelled astrocytes (yellow, arrows) and astrocyte processes (arrowheads) surrounding a blood vessel. **G.** Cofocal images of coronal section through the right temporal cortex, showing GFAP-immunoreactivity in astrocytes (arrows) and in astrocyte processes (arrowheads) infiltrating a leptomeningeal blood vessel. The field in (**H**) shows calpain 1-immunopositive material accumulated in a cortical cell body (arrow), and surrounding a leptomeningeal blood vessel (red colour, arrowheads). The field in (I) shows co-labelling for GFAP and calpain 1-immunoreactivity in a GFAP-positive cell (yellow, arrow), and infiltrating a leptomeningeal blood vessel (yellow, arrowheads). Scale bars: 25 µm (A-I).

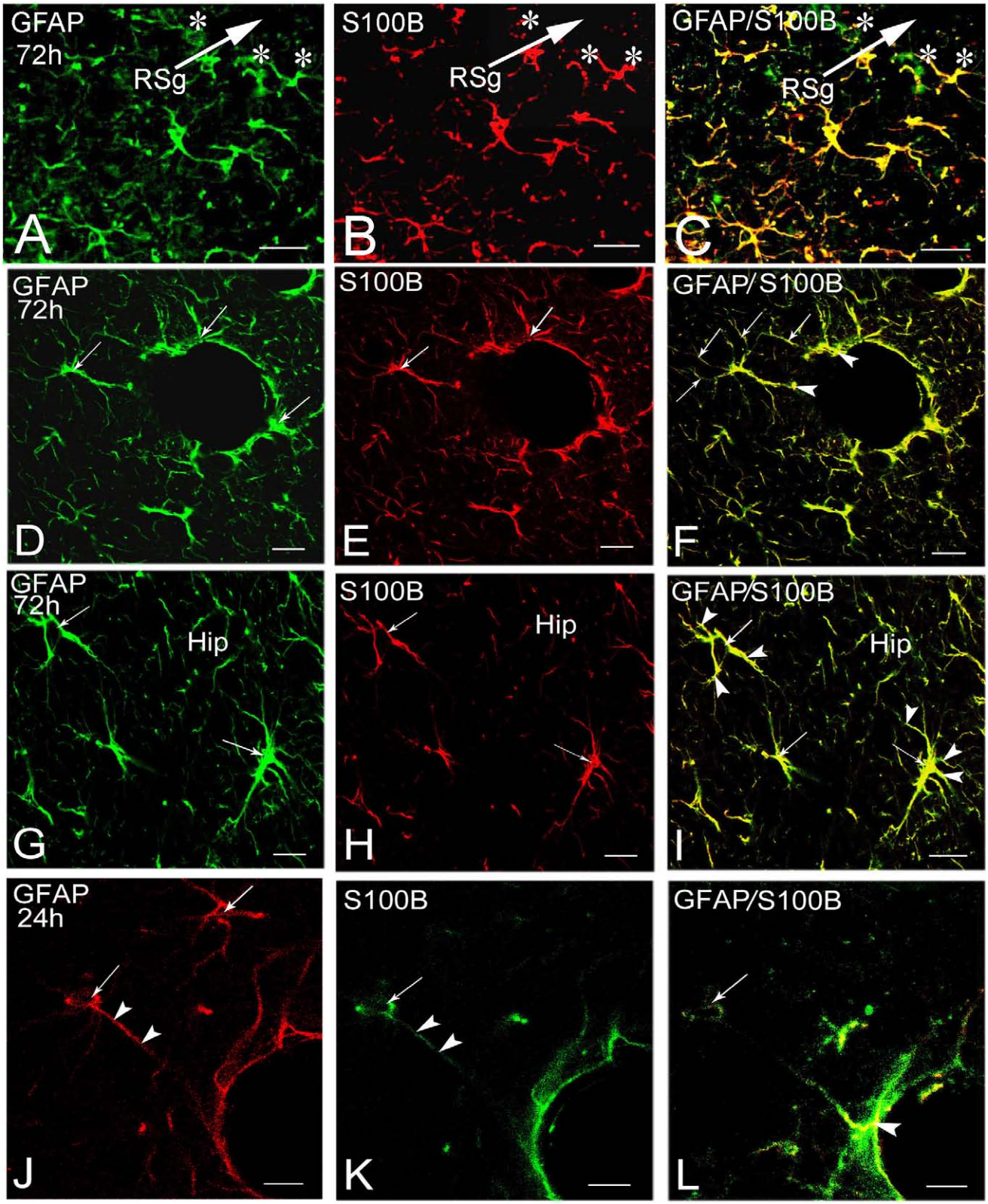

Figure 11. A, B. Confocal images of coronal section of through the RSg, following an injection of Aß1-42 oligomers into the left RSg. The section was processed for the co-localization of GFAP (using FITC, **A**) and S100B (using rhodamine, **B**) proteins. The field in (**C**) shows co-localization of GFAP and S100B proteins (yellow) surrounding the injection site (RSg, arrow), delineated by asterisks. **D-I.** Representative example of sections through the temporal cortex (D-F) and hippocampus (G-I) processed for the co-localization of GFAP (using FITC) and S100B (using rhodamine) after an injection of Aß oligomers into the left RSg at 72h time point. **D-F.** Cofocal images of coronal section through the temporal cortex showing GFAP-immunoreactivity (**D**), S100B-immunopositive material (**E**), and a marked co-labelling of GFAP and S100B proteins (**F**) in the cytoplasm of reactive astrocytes surrounding a blood vessel (arrows). **G-I.** Cofocal images of a coronal section through the ipsilateral hippocampus showing GFAP-immunoreactivity (**G,** arrows) and S100B-immunopositive material (**H**, arrows) in reactive astrocytes. The field in (**I**) shows S100B-immunopositive material accumulated in the cytoplasm (arrows) and in astrocyte processes (arrowheads) of GFAP-positive astrocytes. **J, K.** A representative example of sections through the temporal cortex, processed for the co-localization of GFAP (using rhodamine, J) and S100B (using fluorescein, K), after an injection of Aß oligomers into the left RSg, at an early (24h) time point. Note GFAP- and S100B-immunoreactivity in astrocytes (J, K, arrows) and in astrocyte process (J, K, arrowheads). The field in (**L**) shows S100B-immunopositive material in the cytoplasm (arrow) and in astrocyte process (arrowhead), in close association with a blood vessel. Scale bars: Scale bars: 25 µm (A-L).

Discussion

Beta-amyloid peptide, synaptic pathology, neuronal loss and up-regulation of calpain-1 *in vivo*

A growing body of evidence supports the notion that soluble oligomeric forms of Aß peptide may be the proximate effectors of neuronal injuries and death in the early stages of AD (Haass and Selkoe, 2007; Lacor et al., 2007; Lesné et al., 2006; Walsh and Selkoe, 2007). In the present study, we analyzed the ability of Aß1-42 oligomers to produce synaptic alteration, neuronal degeneration, and other neuropathological features of Aß toxicity *in vivo* in the rat brain. Upon immunohistochemical examination, Aß-oligomer-injected animals exhibited Aß-immunopositive material in neurons in the cerebral cortex and hippocampus during the early (24-72h) phases of Aß toxicity. Additionally Western blotting analysis confirmed that extracellular application of soluble Aß1-42 oligomers into the rat retrosplenial cortex alters the conformation of Aß peptide and induces the accumulation of Aß trimers, tetramers, and multimerizes to higher molecular forms (up to 75-80 kDa) in their brains at an early (24h) time point. This finding is consistent with our previous data showing that extracellular injections of Aß1-42 oligomers into the retrosplenial cortex enhance the formation of Aß peptide intracellularly (Perez et al., 2010), and provides further support for the idea that Aß oligomers and intraneuronal ß-amyloid accumulation play a pathophysiological role in *in vitro* and *in vivo* models of AD (Gouras et al., 2005, 2010; Oddo et al., 2006; Takahashi et al., 2004; Tomiyama et al., 2010). Thus, it appears that this rat model is suitable for studying the contribution of both extracellular Aß oligomers and intracellular Aß accumulation to the neuropathological features induced by Aß toxicity. In this context, here we examined whether loss of synapses occurred following injections of Aß oligomers into the retrosplenial cortex, an important brain area involved in learning and memory processes (Albasser et al., 2007; Lukoyanov and Lukoyanova, 2006; Nestor et al., 2003; Vann and Aggleton, 2002). We analysed markers for small synaptic vesicles, such as synaptophysin, and for large dense-core vesicles, such as chromogranin A. Our findings showed that immunoreactivity for synaptophysin decreased at an early (24h) time point. These findings are supported by studies showing that synaptic dysfunction, and in particular the loss of synaptophysin, in various lines of APP mice occurs before the onset of ß-amyloid plaque pathology (Heinonen et al., 1995; Knobloch et al., 2007; Lacor et al., 2007; Selkoe, 2002), and brain injections of soluble Aß inhibit long-term potentiation in rats (Walsh et al., 2002). Other studies have also demonstrated significant decreases in synaptophysin immunoreactivity in the brains of patients with mild cognitive impairment (Masliah, 2001). Additionally, our immunohistochemical data indicated that injections of Aß1-42 oligomers induced a marked increase in the immunoreactivity for chromogranin A at the centre of the injection of Aß peptide in the early (72h) steps of toxicity induced by Aß oligomers. Thus, our data strongly suggest that, in rats Aß oligomers induce at least two patterns of synaptic dysfunction. These altered synaptic organelles were similar to those characterized previously in AD (Brion et al., 1991; Buttini et al., 2002; Lechner et al., 2004; Masliah et al., 1991). However, which of these synaptic proteins might be responsible for the dysfunction and degeneration of neurons in AD remains a matter of active study and debate. In this regard, further studies should be carried out to evaluate whether the synaptic dysfunction, particularly that associated with synaptophysin and/or with chromogranin A plays a critical role in the neurodegeneration processes induced by Aß.

The most striking feature of AD pathology is neuronal loss. In the present study, we also detected neuronal deficits associated with the injection of Aß oligomers into the retrosplenial cortex of the rat. In APP-Tg mice, the occurrence of neuronal loss has been reported only after an intense development of amyloid plaques (for a review, Duyckaerts et al., 2008). Recently studies, however, have shown that APP$_{E693\Delta}$Tg mice, a mouse model of Aß oligomers, despite their lack of amyloid plaques, exhibit significant neuronal loss in the hippocampal CA3 region at 24 months (Tomiyama et al., 2010). Previous studies have shown that the reduction of neurons *in vivo* is associated with a deposition of Aß deposits (Giovannelli et al., 1995; Gonzalo-Ruiz et al., 2002, 2003; Harkany et al., 1995). To our knowledge, the present contribution is the first report that neuronal loss is induced by Aß oligomers *in vivo* in the rat brain, and our find-

ings provide new insight into the pathogenesis of Aß and strongly suggest that Aß oligomers play a pivotal role throughout the progression of Aß toxicity.

Nevertheless, the molecular events associated with the cell death induced by soluble oligomers of Aß remain only partially defined. One line of evidence has indicated that the neurotoxicity induced by oligomeric forms of Aß1-42 peptide results in a perturbation of Ca^{2+} homeostasis (DeFelice, 2007; Demuro et al., 2005; Ferreiro et al., 2008; Kelly and Ferreira, 2006; Resende et al., 2007; 2008). Evidence has also been gathered to suggest that the disturbance in CA^{2+} homeostasis in turn leads to increased calpain activation (Adamec et al., 2002; Friedrich, 2004; Nixon 2003; Nixon et al., 1994; Raynaud and Marcilhac, 2006; Saito et al., 1993; Wu et al., 2007), and abnormal increases in calpain activity might contribute to Aß-induced neuronal degeneration (Chen and Fernández, 2005; Mathews et al., 2002; Vosler et al., 2008; Wei et al., 2008).

Here, we observed that the injection of oligomers of Aß1-42 results in the proteolysis of three calpain-1 subunits, approximately at positions 80-kDa, a 76-kDa, and at 18-kDa. There are clear indications that, following calcium stimulation, the 80 kDa subunit is partially processed autocatalytically to a 76 kDa fragment, and the Ca^{2+}-dependent autolysis of the small 30-kDa calpain regulatory subunit is processed to the 18-kDa subunit (Goll, 2003). In addition, previous studies have indicated that the 18-kDa calpain regulatory subunit is critical for calpain activity (Goll, 2003; Vosler et al., 2008). Therefore, the increased expression of the small (18kDa) fragment of active calpain-1 observed in Aß1-42-injected animals as compared with that seen in control (Aß42-1) animals points to a close link between soluble oligomers of Aß1-42 and the calpain-1-dependent pathways in the early steps of toxicity induced by Aß. Although the mechanisms underlying the initial activation of calpain are as yet unknown, it is of particular interest to note that an early perturbation of Ca^{2+} homeostasis could play a role in this issue (Friedrich, 2004; Goll, 2003; Nixon, 2003; Vosler et al., 2009).

In addition, we here observed calpain 1-immunopositive material in different cell types, as well as a clear co-localization between calpain-1 and Aß-immunoreactivity in structures-like diffuse aggregate forms. How calpain-1 activity is regulated in cells is still unclear, but previous studies have indicated that the calpain-1 proteolytic system participates in a variety of cellular functions and metabolic process, including APP processing and Aß production (Chen and Fernández, 2005; Mathews et al., 2002; Siman et al., 1990). Some evidence has also shown that calpain is involved in the activation of specific kinases, such as cdk5 (Goñi-Oliver et al., 2009), resulting in a cascade of pro-apoptotic processes through tau phosphorylation (Altznauer et al., 2004). In light of the above, it seems reasonable to assume that Aß1-42 oligomers induce the activation of calpain-1 in different cell types, thereby promoting calcium influx as an early phenomenon involved in the neurotoxicity of Aß and that Aß oligomers might be important in the pathogenesis of AD, as has been indicated previously (LaFerla, 2002; Supnet and Bezprozvanny, 2010).

Calcium-dependent protease, calpain-1, and the calcium-binding protein, S100B, in reactive astrocytes

In our previous study, we showed that extracellular injection of soluble Aß oligomers initiated a rapid increase in GFAP-immunoreactivity and produced a marked increase in the density of a 48kDa fragment of GFAP (Perez et al., 2010). Here, we confirmed our earlier results showing that Aß immunoreactivity is expressed in reactive astrocytes that surround and infiltrate the injection of Aß1-42 peptide into the retrosplenial cortex. Similarly, the present findings show that extracellular injections of Aß1-42 oligomers lead to calpain-1 immunoreactivity, which is normally confined to neurons (Hamakubo et al., 1986; Siman et al., 1985), in reactive astrocytes at an early (24h) time point, increasing at later stages of Aß toxicity. Thus, calpain-1 might be involved in the rapid increase in GFAP-IR in response to Aß toxicity. Furthermore, our results suggest that the reversible (Aß42-1) peptide produces weak calpain-1 immunoreactivity in reactive astrocytes, most likely due to mechanical lesion of the cortical tissue adjacent to the needle tracts. This finding is consistent with previous reports (Du et al., 1999; Fujita et al., 1998; Lee et al., 2000), founding which calpain activation was found in reactive astrocytes in response to brain injury. Additonally, our results show clear a co-localization between GFAP and calpain 1-immunoreactiv-

ity in reactive astrocytes in close association with blood vessels, including those associated with the meninges, as well as in reactive astrocytes surrounding the subventricular zone of the lateral ventricle. The specific implications of the calcium-dependent protease calpain on astrocytosis are not yet known. One line of evidence indicates that the neurotoxicity induced by Aß is primarily mediated by calcium-dependent activation in astrocytes (Abramov et al., 2003; 2004; Rossi and Volterra, 2009). Abnormalities in Ca^{2+} regulation in astrocytes have also been documented in studies of experimental models of AD, suggesting the contributions of these alterations to neuronal dysfunction and cell death in AD (Mattson and Chan, 2003). Since Ca^{2+} waves have been shown to propagate from astrocyte to astrocyte (Kuchibhotla et al., 2009), and from astrocyte to neurons via physical intercellular connections such as gap junctions (Bezzi et al., 2001; Blanc et al., 1998; Nedergaard, 1994), our results suggest that alterations in Ca^{2+} signalling in astrocytes *in vivo* are not confined to the domain of neighbouring synaptic transmission, but may instead elicit larger effects in both astrocytes and neurons, together with a generalized dysfunction in neuron-glia-vascular communications. Complementary to this, other studies have also shown that calpain is involved in the degradation of GFAP in response to brain injury (DeArmond et al., 1983). Indeed, calpain inhibitors have been reported to block proteolysis and the resulting GFAP cleavage, and they decrease reactive gliosis (Du et al., 1999; Gray et al., 2006). Therefore, inhibitors of calpain-1 activity might be useful as potential therapeutic drugs for preventing reactive astrocytosis in response to Aß toxicity.

In addition, our results show that extracellular injections of Aß1-42 oligomers lead to an increase in S100B-immunoreactivity in reactive astrocytes at early stages of Aß toxicity. This finding is consistent with previous reports showing that higher concentrations of the S100B protein, a calcium-binding protein, mediates glial activation predominantly in brain astrocytes (Mori et al., 2010; Ridet et al., 1997, Steiner et al., 2007; Zimmer et al., 1995). An aberrant production of S100B protein has also been observed in brain damage (Mori et al., 2008); in several neurodegenerative diseases including AD (Griffin et al., 1998; Mrak and Griffin, 2001; Van Eldik and Griffin, 1994), and in a transgenic mouse model of AD (Sheng et al., 2000). The S100B protein is thought to produce neuronal damage by causing over-expression of inducible nitric oxide synthase (iNOS) (Hu et al., 1996) and the subsequent release of nitric oxide (NO) from activated astrocytes (Donato, 2001; Hu et al., 1997; Petrova et al., 2000; Rothermundt et al., 2003). Therefore, the subsequent neuronal death might be the result of the oxidative stress generated, at least in part, by astrocytic dysfunction.

In conclusion, the data presented here call for more studies looking at astrogliosis and pathological neuronal alterations as integrated phenomena. In particular, it becomes more and more evident that astrocyte dysfunction cannot be simply considered as a marginal event or late reaction to neuronal injury, but rather as an intrinsic component of the neurodegeneration processes induced by Aß.

Acknowledgements

The authors thank Prof. A.R. Lieberman (University College London) for careful reading of the manuscript, Ms. Pilar Pérez for technical assistance, and Mr. David Jimeno for help with confocal microscopy.

Financial Support: This work was supported by public, competitive grants from Junta de Castilla and León (VA017A10-2) to A.G.-R.

Abbreviation for figures

CA1	field CA1 of Ammon's horn
cg	cingulum
RSa	retrosplenial agranular cortex
RSg	retrosplenial granular cortex
Te	temporal cortex
VL	lateral ventricle

References

Abramov AY, Canevari L, Duchen MR (2003) Changes in intracellular calcium and glutathione in astrocytes as the primary mechanism of amyloid neurotoxicity. *J Neurosci,* 23(12): 5088-5095.

Abramov AY, Canevari L, Duchen MR (2004) Calcium signals induced by amyloid ß peptide and their consequences in neurons and astrocytes in culture. *Biochim Biophys Acta*, 1742: 81-87.

Adamec E, Mohan P, Vonsattel JP, Nixon RA (2002) Calpain activation in neurodegenerative diseases: confo-

cal immunofluorescence study with antibodies specifically recognizing the active form of calpain. *Acta Neuropathol*, 104: 92-104.

Albasser MM, Poirier GL, Warburton EC, Aggleton JP (2007) Hippocampal lesions halve immediate-early gene protein counts in retrosplenial cortex: distal dysfunctions in a spatial memory system. *Eur J Neurosci,* 26:1254-1266.

Altznauer F, Conus S, Cavalli A, Folkers G, Simon HU (2004) Calpain-1 regulates Bax and subsequent Smac-dependent caspase-3 activation in neutrophil apoptosis. *J Biol Chem,* 279(7): 5947-5957.

Akiyama H, Barger S, Barnum S, Bradt B, Bauer J, Cole GM, Cooper NR, Eikelenboom P, Emmerling M, Fiebich Bl, Finch CE, Frautschy S, Griffin WS, Hampel H, Hull M, Landreth G, Lue L, Mrak R, Mackenzie Ir, Mcgeer PL, O'banion Mk, Pachter J, Pasinetti G, Plata-Salaman C, Rogers J, Rydel R, Shen Y, Streit W, Strohmeyer R, Tooyoma I, Van Muiswinkel FL, Veerhuis R, Walker D, Webster S, Wegrzyniak B, Wenk G, Wyss-Coray T (2000) Inflammation and Alzheimer's disease. *Neurobiol Aging,* 21: 383-421.

Araque A, Carmignoto G, Haydon PG (2001) Dynamic signalling between astrocytes and neurons. *Annu Rev Physiol,* 63: 795-813.

Arevalo-Serrano J, Sanz-Anquela JM, Gonzalo-Ruiz A (2008) Beta-amyloid peptide-induced modifications in α7 nicotinic acetylcholine receptor immunoreactivity in the hippocampus of the rat. *Brain Res Bull,* 75: 134-143.

Berridge MJ (2010) Calcium hypothesis of Alzheimer's disease. *Pflugers Arch*, 459(3): 441-449.

Bezzi P, Domercq M, Vesce S, Volterra A (2001) Neuron-astrocyte cross-talk during synaptic transmission: physiological and neuropathological implications. *Prog Brain Res*, 132: 255-265.

Blanc EM, Bruce-Keller AJ, Mattson MP (1998) Astrocytic gap junctional communication decreases neuronal vulnerability to oxidative stress-induced disruption of Ca^{2+} homeostasis and cell death. *J Neurochem*, 70(3): 958-970.

Brion JP, Couck AM, Bruce M, Anderton B, Flament-Durand J (1991) Synaptophysin and chromogranin A immunoreactivities in senile plaques of Alzheimer's disease. *Brain Res,* 539(1): 143-150.

Buttini M, Yu GQ, Shockley K, Huang Y, Jones B, Masliah E, Mallory M, Yeo T, Longo FM, Mucke L (2002) Modulation of Alzheimer-like synaptic and cholinergic deficits in transgenic mice by human apolipoprotein E depends on isoform, aging, and over expression of amyloid beta peptides but not on plaque formation. *J Neurosci,* 22(24): 10539-10548.

Chen M, Fernandez L (2005) Mu-calpain is functionally required for alpha-processing of Alzheimer's beta-amyloid precursor protein. *Biochem Biophys Res Commun* 330(3): 714-721.

Cleary JP, Walsh DM, Hofmeister JJ, Shankar GM, Kuskowski MA, Selkoe DJ, Ashe K. (2005). Natural oligomers of the amyloid-beta protein specifically disrupt cognitive function. *Nat Neurosci*, 8: 79-84.

Dearmond SJ, Fajardo M, Naughton SA, Eng LF (1983) Degradation of glial fibrillary acidic protein by a calcium dependent proteinase: an electroblot study. *Brain Res,* 262(2): 275-282.

Defelice FG, Velasco PT, Lambert MP, Viola K, Fernández SJ, Ferreira ST, Klein WL (2007) Abeta oligomers induce neuronal oxidative stress through an N-methyl-D-aspartate receptor-dependent mechanism that is blocked by the Alzheimer drug memantine. *J Biol Chem,* 282: 11590-11601.

Demuro A, Mina E, Kayed R, Milton SC, Parker I, Glabe CG (2005) Calcium dysregulation and membrane disruption as a ubiquitous neurotoxic mechanism of soluble amyloid oligomers. *J Biol Chem,* 280: 17294-17300.

Domenici MR, Paradisi S, Sacchetti B, Gaudi S, Balduzzi M, Bernardo A, Ajmone-Cat MA, Minghetti L, Malchiodi-Albedi F (2002) The presence of astrocytes enhances beta amyloid-induced neurotoxicity in hippocampal cell cultures. *J Physiol,* 96: 313-316.

Donato R (2001) S100: a multigenic family of calcium-modulated proteins of the EF-hand type with intracellular and extracellular functional roles. *Int J Biochem Cell Biol,* 33: 637-668.

Du S, Rubin A, Klepper S, Barrett C, Kim YC, Rhim HW, Lee EB, Park CW, Markelonis GJ, Oh TH (1999) Calcium influx and activation of calpain I mediate acute reactive gliosis in injured spinal cord. *Exp Neurol,* 157: 96-105.

Duyckaerts C, Potier MC, Delatour B (2008) Alzheimer disease models and human neuropathology: similarities and differences. *Acta Neuropathol*, 115(1): 5-38.

Ferreiro E, Oliveira CR, Pereira CM (2008) The release of calcium from the endoplasmic reticulum induced by amyloid-beta and prion peptides activates the mitochondrial apoptotic pathway. *Neurobiol Dis,* 30(3): 331-342.

Friedrich P (2004) The intriguing Ca^{2+} requirement of calpain activation. *Biochem Biophys Res Commun*, 323(4): 1131-1133.

Fujita K, Yamauchi M, Matsui T, Titani K, Takahashi H, Kato T, Isomura G, Ando M, Nagata Y (1998). Increase of glial fibrillary acidic protein fragments in the spinal cord of motor neuron degeneration mutant mouse. *Brain Res,* 785: 31-40.

Giovannelli L, Casamenti F, Scali C, Bartolini L, Pepeu G (1995) Differential effects of amyloid peptides beta-(1-40) and beta-(25-35) injections into the rat nucleus basalis. *Neuroscience*, 66: 1113-1117.

Goll DE (2003) The calpain system. *Physiol Rev,* 83: 731-801.

Gong Y, Chang L, Viola KL, Lacor PN, Lambert MP, Finch CE, Krafft GA, Klein WL (2003) Alzheimer's disease-affected brain: presence of oligomeric Abeta ligands (ADDLs) suggests a molecular basis for reversible memory loss. *Proc Natl Acad Sci USA* 100(18): 10417-10422.

González I, Arévalo-Serrano J, Pérez JL, Gonzalo P, Gonzalo-Ruiz A (2008) Effects of Beta-amyloid peptide on the density of M2 muscarinic acetylcholine receptor immunoreactivity in the hippocampus of the rat. *Neuropathol Appl Neurobiol*, 34: 506-522.

Gonzalo-Ruiz A, Sanz JM (2002) Alteration of cholinergic, excitatory amino acid and neuropeptide markers in the septum-diagonal band complex following injections of fibrillar ß-amyloid protein into the retrosplenial cortex of the rat. *Eur J Anat*, 6: 58–71.

Gonzalo-Ruiz A, González I, Sanz-Anquela, JM (2003) Effects of ß-amyloid protein on serotoninergic, noradrenergic, and cholinergic markers in neurons of the

pontomesencephalic tegmentum in the rat. *J Chem Neuroanat,* 26: 153–170.

Goñi-Oliver P, Avila J, Hernandez F (2009) Memantine Inhibits Calpain-Mediated Truncation of GSK-3 Induced by NMDA: Implications in Alzheimer's disease. *J Alzheimers Dis,* 18(4): 843-848.

Gouras GK, Almeida CG, Takahashi RH (2005) Intraneuronal Abeta accumulation and origin of plaques in Alzheimer's disease. *Neurobiol Aging,* 26(9): 1235-1244.

Gouras GK, Tampellini D, Takahashi RH, Capetillo-Zarate E (2010) Intraneuronal beta-amyloid accumulation and synapse pathology in Alzheimer's disease. *Acta Neuropathol,* 119(5): 523-541.

Gray BC, Skipp P, O'connor VM, Perry VH (2006) Increased expression of glial fibrillary acidic protein fragments and mu-calpain activation within the hippocampus of prion-infected mice. *Biochem Soc Trans*, 34: 51-54.

griffin WS, Sheng JG, Royston MC, Gentleman SM, Mckenzie JE, Graham DI, Roberts GW, Mrak RE (1998) Glial-neuronal interactions in Alzheimer's disease: the potential role of a 'cytokine cycle' in disease progression. *Brain Pathol*, 8: 65-72.

Haass C, Selkoe DJ (2007) Soluble protein oligomers in neurodegeneration: lessons from the Alzheimer's amyloid beta-peptide. *Nat Rev Mol Cell Biol*, 8: 101-112.

Hamakubo T, Kannagi R, Murachi T, Matus A (1986) Distribution of calpains I and II in rat brain. *J Neurosci,* 6(11): 3103-3111.

Hardy J, Selkoe DJ (2002) The amyloid hypothesis of Alzheimer's disease: progress and problems on the road to therapeutics. *Science*, 297: 353-356.

Harkany t, z. Lengyel, k. Soós, b. Penke, P.G.M. Luiten, k. Gulya K (1995). Cholinotoxic effects of ß-amyloid (1-42) peptide on cortical projections of the rat nucleus basalis magnocellularis. *Brain Res,* 685: 71-75.

Heinonen O, Soininen H, Sorvari H, Kosunen O, Paljärvi L, Koivisto E, Riekkinen PJ (1995) Loss of synaptophysin-like immunoreactivity in the hippocampal formation is an early phenomenon in Alzheimer's disease. *Neuroscience*, 64(2): 375-384.

Hernandez CM, Kayed R, Zheng H, Sweatt JD, Dineley KT (2010) Loss of alpha7 nicotinic receptors enhances beta-amyloid oligomer accumulation, exacerbating early-stage cognitive decline and septohippocampal pathology in a mouse model of Alzheimer's disease. *J Neurosci*, 30(7): 2442-2453.

Hu J, Castets F, Guevara JL, Van Eldik LJ (1996) S100 beta stimulates inducible nitric oxide synthase activity and mRNA levels in rat cortical astrocytes. *J Biol Chem*, 271(5): 2543-2547.

Hu J, Ferreira A, Van Eldik LJ (1997) S100beta induces neuronal cell death through nitric oxide release from astrocytes. *J Neurochem,* 69(6): 2294-2301.

Johnstone M, Gearing AJ, Miller KM (1999) A central role for astrocytes in the inflammatory response to beta-amyloid; chemokines, cytokines and reactive oxygen species are produced. *J Neuroimmunol,* 93: 182-193.

Kelly BL, Ferreira A (2006) Beta-amyloid-induced dynamin 1 degradation is mediated by N-methyl-D-aspartate receptors in hippocampal neurons. *J Biol Chem*, 281: 28079-29089.

Klein WL (2002) Aß toxicity in Alzheimer's disease: globular oligomers (ADDLs) as new vaccine and drug targets. *Neurochemistry International*, 41: 345-352.

Knobloch M, Farinelli M, Konietzko U, Nitsch RM, Mansuy IM (2007) Abeta oligomer-mediated long-term potentiation impairment involves protein phosphatase 1-dependent mechanisms. *Neurosci*, 27(29): 7648-7653.

Kokubo H, Kayed R, Glabe CG, Yamaguchi H (2005) Soluble Aß oligomers ultrastructurally localize to cell processes and might be related to synaptic dysfunction in Alzheimer's disease brain. *Brain Res*, 1031: 222-228.

Korolainen MA, Auriola S, Nyman TA, Alafuzoff I, Pirttilä T (2005) Proteomic analysis of glial fibrillary acidic protein in Alzheimer's disease and aging brain. *Neurobiol Dis,* 20(3): 858-870.

Kuchibhotla KV, Lattarulo CR, Hyman BT, Bacskai BJ (2009) Synchronous hyperactivity and intercellular calcium waves in astrocytes in Alzheimer mice. *Science*, 323: 1211-1215.

Lacor PN, Buniel MC, Furlow PW, Clemente AS, Velasco PT, Wood M, Viola KL, Klein WL (2007) Abeta oligomers-induced aberrations in synapse composition, shape, and density provide a molecular basis for loss of connectivity in Alzheimer's disease. *J Neurosci,* 27(4): 796-807.

Laferla FM (2002) Calcium dyshomeostasis and intracellular signalling in Alzheimer's disease. *Nat Rev Neurosci*, 3: 862-872.

Lebart MC, Benyamin Y (2006) Calpain involvement in the remodelling of cytoskeletal anchorage complexes. *FEBS J,* 272: 3415-3426.

Lechner T, Adlassnig C, Humpel C, Kaufmann WA, Maier H, Reinstadler-Kramer K, Hinterhölzl J, Mahata SK, Jellinger KA, Marksteiner J (2004) Chromogranin peptides in Alzheimer's disease. *Exp Gerontol*, 39(1): 101-113.

Lee YB, Du S, Rhim H, Lee EB, Markelonis GJ, Oh TH (2000) Rapid increase in immunoreactivity to GFAP in astrocytes in vitro induced by acidic pH is mediated by calcium influx and calpain I. *Brain Res,* 864: 220-229.

Lesné S, Koh MT, Kotilinek L, Kayed R, Glabe CG, Yang A, Gallagher M, Ashe KH (2006) A Specific amyloid-ß protein assembly in the brain impairs memory. *Nature,* 440: 352-357.

Levey AI, Bolam JP, Rye DB, Hallanger AE, Demuth RM, Mesulam MM, Wainer BH (1986) A light and electron microscopic procedure for sequential double antigen localization using diaminobenzidine and benzidine dihydrochloride. *J Histochem Cytochem*, 34: 1449-1457.

Lukoyanov NV, Lukoyanova EA (2006) Retrosplenial cortex lesions impair acquisition of active avoidance while sparing fear-based emotional memory. *Behav Brain Res*, 173(2): 229-236.

Malchiodi-Albedi F, Domenici MR, Paradisi S, Bernardo A, Ajmone-Cat Ma, Minghetti L. (2001) Astrocytes contribute to neuronal impairment in ßA toxicity increasing apoptosis in rat hippocampal neurons. *Glia*, 34: 68-72.

Mark RJ, Keller JN, Kruman I, Mattson MP (1997) Basic FGF attenuates amyloid beta-peptide-induced oxidative stress mitochondrial dysfunction, and impairment of Na^+/K^+-ATPase activity in hippocampal neurons. *Brain Res,* 756: 205-214.

Masliah E (2001) Recent advances in the understanding of the role of synaptic proteins in Alzheimer's Diseases and other neurodegenerative disorders. *J Alzheimers Dis,* 3(1): 121-129.

Masliah E, Hansen L, Albright T, Mallory M, Terry RD (1991) Immunoelectron microscopic study of synaptic pathology in Alzheimer's disease. *Acta Neuropathol,* 81(4): 428-433.

mathews PM, Jiang Y, Schmidt Sd, Grbovic OM, Mercken M, Nixon RA (2002) Calpain activity regulates the cell surface distribution of amyloid precursor protein. Inhibition of calpains enhances endosomal generation of beta-cleaved C-terminal APP fragments. *J Biol Chem,* 277(39): 36415-36424.

Mattson MP, Chan SL (2003) Neuronal and glial calcium signalling in Alzheimer's disease. *Cell Calcium,* 34: 385-397.

McGeer PL, McGeer EG (2001) Inflammation, auto-toxicity and Alzheimer disease. *Neurobiol Aging*, 22: 799-809.

Meda L, Baron P, Scarlato G (2001) Glial activation in Alzheimer's disease: the role of Abeta and its associated proteins. *Neurobiol Aging*, 22: 885-893.

Mori T, Koyama N, Arendash Gw, Horikoshi-Sakuraba Y, Tan J, Town T (2010) Overexpression of human S100B exacerbates cerebral amyloidosis and gliosis in the Tg2576 mouse model of Alzheimer's disease. *Glia,* 58(3): 300-314.

Mori T, Tan J, Arendash Gw, Koyama N, Nojima Y, Town T (2008) Over expression of human S100B exacerbates brain damage and periinfarct gliosis after permanent focal ischemia. *Stroke,* 39(7): 2114-2121.

Mrak RE, Griffin WS (2005) Glia and their cytokines in progression of neurodegeneration. *Neurobiol Aging,* 26 (3): 349-354

Mucke L, Masliah E, Yu G Q, Mallory M, Rockenstein Em, Tatsuno G, Hu K, Kholodenko D, Johnson-Wood K, McConlogue L (2000) High-level neuronal expression of Aß1-42 in wild-type human amyloid protein precursor transgenic mice: synaptotoxicity without plaque formation. *J Neurosci,* 20: 4050-4058.

Nedergaard M (1994) Direct signalling from astrocytes to neurons in cultures of mammalian brain cells. *Science*, 263(5154): 1768-1771.

Nestor PJ, Fryer TD, Ikeda M, Hodges JR (2003) Retrosplenial cortex (BA29/30) hypometabolism in mild cognitive impairment (prodromal Alzheimer's disease). *Eur J Neurosci*, 18(9): 2663-2667.

Nixon Ra (2003) The calpains in aging and aging-related diseases. *Ageing Res Rev*, 2: 407-418.

Nixon RA, Saito KI, Grynspan F, Griffin WR, Katayama S, Honda T, Mohan PS, Shea TB, Beermann M (1994) Calcium-activated neutral proteinase (calpain) system in aging and Alzheimer's disease. *Ann N Y Acad Sci*, 747: 77-91.

Oddo S, Caccamo A, Tran L, Lambert MP, Glabe CG, Klein WL, Laferla FM (2006) Temporal profile of amyloid-beta (Abeta) oligomerization in an in vivo model of Alzheimer disease. A link between Abeta and tau pathology. *J Biol Chem,* 281: 1599-1604.

Paxinos G, Watson C (1986) The Rat Brain in Stereotaxic Coordinates. Academic Press, New York.

Perez JL, Carrero I, Gonzalo P, Arévalo-Serrano J, Sanz-Anquela JM, Ortega J, Rodríguez J, Gonzalo-Ruiz A (2010) Soluble oligomeric forms of beta-amyloid (Aß) peptide stimulate Aß production via astrogliosis in the rat brain. *Exp Neurol*, 223: 410-421.

Petrova TV, Hu J, Van Eldik LJ (2000) Modulation of glial activation by astrocyte-derived protein S100B: differential responses of astrocyte and microglial cultures. *Brain Res*, 853(1): 74-80.

ramonet D, Rodríguez MJ, Puglisi M, Mahy N (2004) Putative glucosensing property in rat and human activated microglia. *Neurobiol Dis,* 17:1-9.

Raynaud F, Marcilhac A (2006) Implication of calpain in neuronal apoptosis. A possible regulation of Alzheimer's disease. *FEBS J*, 273: 3437-3443.

Resende R, Pereira C, Agostinho P, Vieira AP, Malva JO, Oliveira Cr (2007) Susceptibility of hippocampal neurons to Abeta peptide toxicity is associated with perturbation of Ca^{2+} homeostasis. *Brain Res,* 1143: 11-21.

Resende R, Ferreiro E, Pereira C, Resende de Oliveira C (2008) Neurotoxic effect of oligomeric and fibrillar species of amyloid-beta peptide 1-42: involvement of endoplasmic reticulum calcium release in oligomer-induced cell death. *Neuroscience*, 155: 725-737.

Reymond I, Almarghini K, Tappaz M (1996) Immunocytochemical localization of cysteine sulfinate decarboxylase in astrocytes in the cerebellum and hippocampus: a quantitative double immunofluorescence study with glial fibrillary acidic protein and S-100 protein. *Neuroscience*, 75(2): 619-633.

Ridet JL, Malhotra SK, Privat A, Gage FH (1997) Reactive astrocytes: cellular and molecular cues to biological function. *Trends Neurosci*, 20(12): 570-577.

Riederer IM, Schiffrin M, Kovari E, Bouras C, Riederer BM (2009) Ubiquitinationand cysteine nitrosylation during aging and Alzheimer's disease. *Brain Res Bul*l, 80: 233-241.

Rodríguez JJ, Olabarria M, Chvatal A, Verkhratsky A (2009) Astroglia in dementia and Alzheimer's disease. Cell Death Differ, 16(3): 378-385.

Rossi D, Volterra A (2009) Astrocytic dysfunction: insight on the role in neurodegeneration. *Brain Res Bull,* 80: 224-232.

Rothermundt M, Peters M, Prehn JH, Arolt V (2003) S100B in brain damage and neurodegeneration. *Microsc Res Tech,* 60(6): 614-632.

Saito K, Elce JS, Hamos JE, Nixon RA (1993) Widespread activation of calcium-activated neutral proteinase (calpain) in the brain in Alzheimer disease: a potential molecular basis for neuronal degeneration. *Proc Natl Acad Sci USA,* 90: 2628-2632.

Selkoe DJ (2002) Alzheimer's disease is a synaptic failure. *Science*, 298:789-791.

Selkoe DJ (2008) Soluble oligomers of the amyloid beta-protein impair synaptic plasticity and behavior. *Behav Brain Res,* 192: 106-113.

Selkoe DJ, Schenk D (2003) Alzheimer's disease: molecular understanding predicts amyloid based therapeutics. *Annu Rev Pharmacol Toxicol,* 43: 545-584.

Sheng JG, Mrak RE, Bales KR, Cordell B, Paul SM, Jones RA, Woodward S, Zhou XQ, Mcginness JM, Griffin WS (2000) Overexpression of the neuritotrophic cytokine S100beta precedes the appearance of neuritic beta-amyloid plaques in APPV717F mice. *J Neurochem,* 74(1): 295-301.

Siman R, Card JP, Davis LG (1990) Proteolytic processing of beta-amyloid precursor by calpain I. *J Neurosci,* 10(7): 2400-2411.

Siman R, Gall C, Perlmutter LS, Christian C, Baudry M, Lynch G (1985) Distribution of calpain I, an enzyme

associated with degenerative activity, in rat brain. *Brain Res*, 347(2): 399-403.

Simpson JE, Ince PG, Lace G, Forster G, Shaw PJ, Matthews F, Sava G, Brayne C, Wharton SB (2010) Astrocyte phenotype in relation to Alzheimer-type pathology in the ageing brain. Neurobiol Aging, 31(4): 578-590.

Steiner J, Bernstein HG, Bielau H, Berndt A, Brisch R, Mawrin C, Keilhoff G, ogerts B (2007) Evidence for a wide extra-astrocytic distribution of S100B in human brain. *BMC Neurosci*, 8: 2

Supnet C, Bezprozvanny I (2010) The dysregulation of intracellular calcium in Alzheimer disease. *Cell Calcium*, 47(2):183-189.

Takahashi, RH, Almeida, CG, Kearney, PF, Yu, F, Lin, MT, Milner, TA, Gouras, GK (2004) Oligomerization of Alzheimer's beta-amyloid within processes and synapses of cultured neurons and brain. *J Neurosci,* 24: 3592-3599.

Takuma K, Baba A, Matsuda T (2004) Astrocyte apoptosis: implications for neuroprotection. Prog Neurobiol, 72: 111-127.

Tampellini D, Capetillo-Zarate E, Dumont M, Huang Z, Yu F, Lin MT, Gouras GK (2010) Effects of synaptic modulation on beta-amyloid, synaptophysin, and memory performance in Alzheimer's disease transgenic mice. *J Neurosci,* 30(43): 14299-14304.

Tomiyama T, Matsuyama S, Iso H, Umeda T, Takuma H, Ohnishi K, Ishibashi K, Teraoka R, Sakama N, Yamashita T, Nishitsuji K, Ito K, Shimada H, Lambert MP, Klein WL, Mori H (2010) A mouse model of amyloid ß oligomers: their contribution to synaptic alteration, abnormal tau phosphorylation, glial activation, and neuronal loss *in vivo*. *J Neurosci*, 30(14): 4845-4856.

Town T, Nikolic V, Tan J (2005) The microglial «activation» continuum: from innate to adaptive responses. *J Neuroinflammation,* 2: 24. doi: 10.1186/1742-2094-2-24.

Van Eldik LJ, Griffin WS (1994) S100 beta expression in Alzheimer's disease: relation to neuropathology in brain regions. *Biochim Biophys Acta,* 1223(3): 398-403.

Vann SD, Aggleton JP (2002) Extensive cytotoxic lesions of the rat retrosplenial cortex reveals consistent deficits on tasks that tax allocentric spatial memory. *Behav Neurosci,* 116: 85-94.

Vosler PS, Brennan CS, Chen J (2008) Calpain-Mediated Signalling Mechanisms in neuronal injury and neurodegeneration. *Mol. Neurobiol*, 38:78-100.

Vosler PS, Sun D, Wang S, Gao Y, Kintner DB, Signore Ap, Cao G, Chen J (2009) Calcium dysregulation induces apoptosis-inducing factor release: cross-talk between PARP-1- and calpain-signalling pathways. *Exp Neurol*, 218(2): 213-220.

Walsh DM, Selkoe DJ (2007) Beta oligomers - a decade of discovery. *J Neurochem*, 101: 1172-1184.

Walsh DM, Klyubin I, Fadeeva JV, Cullen Wk, Anwyl R, Wolfe MS, Rowan MJ, Selkoe DJ (2002) Naturally secreted oligomers of amyloid beta protein potently inhibit hippocampal long-term ostentation in vivo. *Nature,* 416: 535-539.

Wei Z, Song MS, Mactavish D, Jhamandas JH, Kar S (2008) Role of calpain and caspase in ß-amyloid-induced cell death in rat primary septal cultures neurons. *Neuropharmacology,* 54: 721-733.

Wu Hy, Tomizawa K, Matsui H (2007) Calpain-calcineurin signalling in the pathogenesis of calcium-dependent disorder. *Acta Med Okayama,* 61: 123-137.

Zimmer DB, Cornwall EH, Landar A, Song W (1995) The S100 protein family: history, function, and expression. *Brain Res Bull,* 37(4): 417-429.